

## MIT Open Access Articles

*GPS velocity field for the Tien Shan and surrounding regions*

The MIT Faculty has made this article openly available. **Please share** how this access benefits you. Your story matters.

**Citation:** Zubovich, Alexander V. et al. "GPS Velocity Field for the Tien Shan and Surrounding Regions." *Tectonics* 29.6 (2010). ©2012. American Geophysical Union.

**As Published:** <http://dx.doi.org/10.1029/2010tc002772>

**Publisher:** American Geophysical Union (AGU)

**Persistent URL:** <http://hdl.handle.net/1721.1/75344>

**Version:** Final published version: final published article, as it appeared in a journal, conference proceedings, or other formally published context

**Terms of Use:** Article is made available in accordance with the publisher's policy and may be subject to US copyright law. Please refer to the publisher's site for terms of use.



## GPS velocity field for the Tien Shan and surrounding regions

Alexander V. Zubovich,<sup>1,2</sup> Xiao-qiang Wang,<sup>3</sup> Yuri G. Scherba,<sup>4</sup>  
Gennady G. Schelochkov,<sup>1</sup> Robert Reilinger,<sup>5</sup> Christoph Reigber,<sup>2,6</sup> Olga I. Mosienko,<sup>1,2</sup>  
Peter Molnar,<sup>7</sup> Wasili Michajljow,<sup>2,6</sup> Vladimir I. Makarov,<sup>8</sup> Jie Li,<sup>3,9</sup> Sergey I. Kuzikov,<sup>1</sup>  
Thomas A. Herring,<sup>5</sup> Michael W. Hamburger,<sup>10</sup> Bradford H. Hager,<sup>5</sup> Ya-min Dang,<sup>11</sup>  
Vitaly D. Bragin,<sup>1</sup> and Rinat T. Beisenbaev<sup>12</sup>

Received 30 July 2010; revised 30 September 2010; accepted 15 October 2010; published 23 December 2010.

[1] Measurements at ~400 campaign-style GPS points and another 14 continuously recording stations in central Asia define variations in their velocities both along and across the Kyrgyz and neighboring parts of Tien Shan. They show that at the longitude of Kyrgyzstan the Tarim Basin converges with Eurasia at  $20 \pm 2$  mm/yr, nearly two thirds of the total convergence rate between India and Eurasia at this longitude. This high rate suggests that the Tien Shan has grown into a major mountain range only late in the evolution of the India–Eurasia collision. Most of the convergence between Tarim and Eurasia within the upper crust of the Tien Shan presumably occurs by slip on faults on the edges of and within the belt, but 1–3 mm/yr of convergence is absorbed farther north, at the Dzungarian Alatau and at a lower rate with the Kazakh platform to the west. The Tarim Basin is thrust beneath the Tien Shan at ~4–7 mm/yr. With respect to Eurasia, the Ferghana Valley rotates counterclockwise at  $\sim 0.7^\circ \text{ Myr}^{-1}$  about an axis at the southwest end of the valley. Thus, GPS data place a bound of ~4 mm/yr on the rate of crustal shortening across the Chatkal and neighboring ranges

on the northwest margin of the Ferghana Valley, and they limit the present-day slip rate on the right-lateral Talas–Ferghana fault to less than ~2 mm/yr. GPS measurements corroborate geologic evidence indicating that the northern margin of the Pamir overthrusts the Alay Valley and require a rate of at least 10 and possibly 15 mm/yr. **Citation:** Zubovich, A. V., et al. (2010), GPS velocity field for the Tien Shan and surrounding regions, *Tectonics*, 29, TC6014, doi:10.1029/2010TC002772.

### 1. Introduction

[2] Whereas slip on a single fault at a boundary between oceanic plates accommodates virtually all relative motion between the adjacent plates, intracontinental deformation commonly occurs by widespread deformation and slip on numerous faults. This form of deformation is particularly apparent where mountain ranges have been built in intracontinental settings, such as that in which the Rocky Mountains of the western United States developed in late Cretaceous and early Cenozoic (Laramide) time.

[3] The Tien Shan serves as the prototypical active intracontinental mountain belt. Separate ranges, bounded on one or both sides by reverse faults and with intermontane basins between them, collectively form a belt of widespread deformation and abundant seismicity far from boundaries of the major plates (Figure 1). Such belts typify active deformation elsewhere in Asia, such as in Mongolia or on the northeastern margin of the Tibetan Plateau, and they characterize the separate ranges that form the Andes in parts of Colombia, Venezuela, Peru, and Argentina. In active intracontinental belts, several faults are concurrently active; no single fault defines a plate boundary. Lateral continuity of individual ranges, however, can be short, only 100–200 km, and slip rates on faults within the belts vary along strike.

[4] The Tien Shan illustrates these features. Both field observations of active faulting [e.g., *Abdrakhmatov et al.*, 2007; *Chedia*, 1986; *Laverov and Makarov*, 2005; *Makarov*, 1977; *Makarov et al.*, 2010; *Sadybakasov*, 1990; *Shultz*, 1948; *Thompson et al.*, 2002] and fault plane solutions of moderate earthquakes [e.g., *Ghose et al.*, 1998; *Maggi et al.*, 2000; *Nelson et al.*, 1987; *Tapponnier and Molnar*, 1979] demonstrate largely reverse faulting, in some cases with modest but not negligible strike-slip components. Four earthquakes with magnitudes greater than approximately 8 have occurred within the Tien Shan since 1889 [e.g.,

<sup>1</sup>Research Station of the Russian Academy of Sciences, Bishkek, Kyrgyzstan.

<sup>2</sup>Department of Technical Infrastructures and Data Management, Central Asian Institute for Applied Geosciences, Bishkek, Kyrgyzstan.

<sup>3</sup>Earthquake Administration of the Xinjiang Uygur Autonomous Region, Urumqi, China.

<sup>4</sup>National Center of Space Researches and Technologies, National Space Agency of the Republic of Kazakhstan, Almaty, Kazakhstan.

<sup>5</sup>Department of Earth, Atmospheric, and Planetary Sciences, Massachusetts Institute of Technology, Cambridge, Massachusetts, USA.

<sup>6</sup>Department 1, Deutsches GeoForschungsZentrum, Potsdam, Germany.

<sup>7</sup>Department of Geological Sciences and Cooperative Institute for Research in Environmental Sciences, University of Colorado, Boulder, Colorado, USA.

<sup>8</sup>Institute of Environmental Geosciences, Russian Academy of Sciences, Moscow, Russia.

<sup>9</sup>Research Center of Space Science and Technology, China University of Geosciences, Wuhan, China.

<sup>10</sup>Department of Geological Sciences, Indiana University, Bloomington, Indiana, USA.

<sup>11</sup>Chinese Academy of Surveying and Mapping, Beijing, China.

<sup>12</sup>Seismological Experimental-Methodical Expedition, Almaty, Kazakhstan.

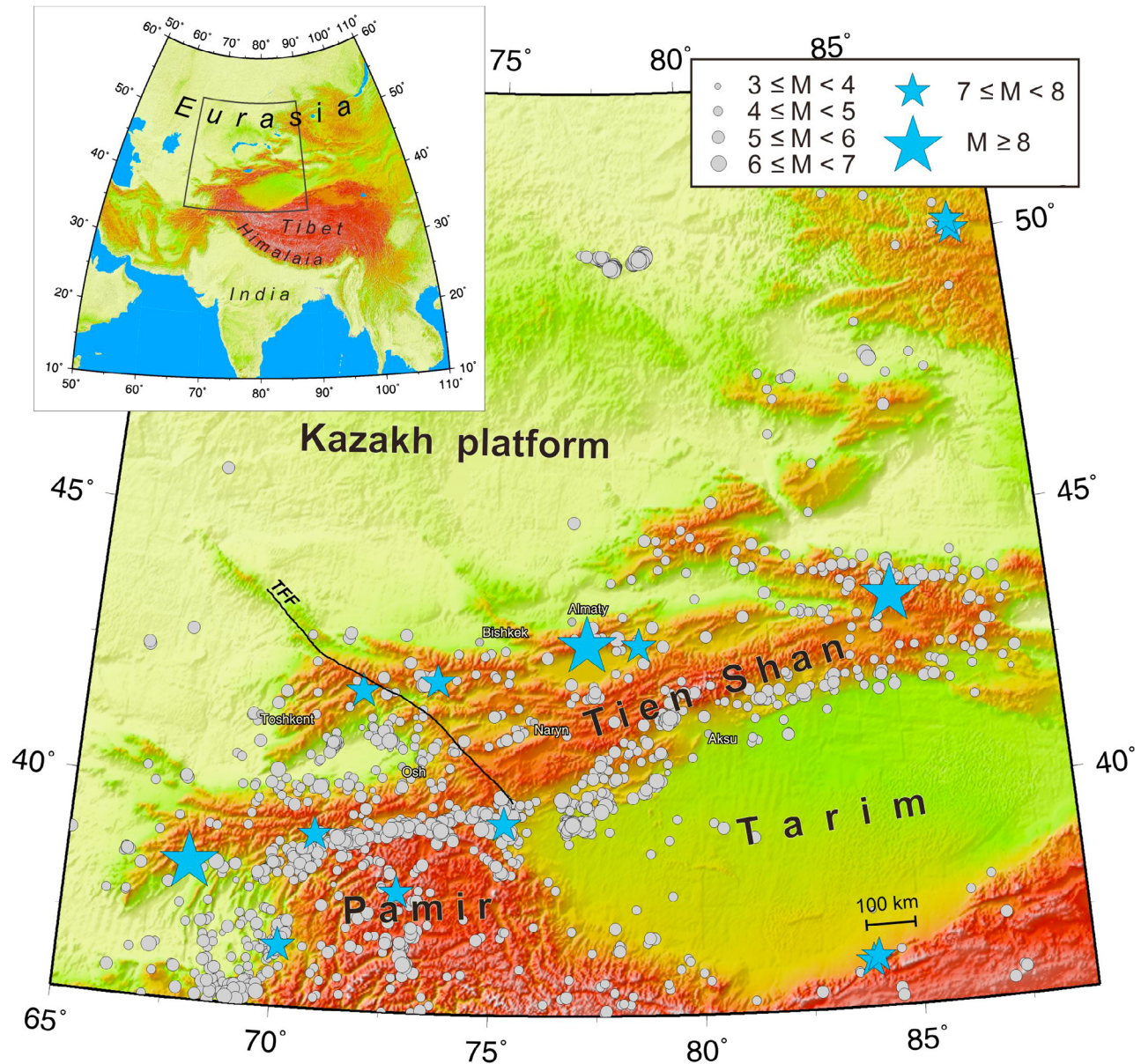


**Figure 1.** Map of the central Tien Shan and surroundings showing topography, shallow-focus seismicity, selected cities, and the trace of the Talas-Ferghana fault (TFF). Gray circles show events with precise locations given and updated by *Engdahl et al.* [1998], and blue stars show events with  $7 \leq M < 8$  and  $M \geq 8$  from *Molnar and Deng* [1984]. The inset shows the regional setting of the Tien Shan.

*Kondorskaya and Shebalin, 1977; Gu et al., 1989; Molnar and Ghose, 2000; Richter, 1958; Savarenskii et al., 1962*. Studies of Quaternary faulting demonstrate slip at rates of 1 to 4 mm/yr on several approximately parallel faults that divide the belt into blocks tens of kilometers in width [e.g., *Abdrakhmatov et al., 2007; Makarov, 1977; Thompson et al., 2002*]. Deep basins with 2000 m or more of late Cenozoic sediment lie between ranges [e.g., *Cobbold et al., 1996; Laverov and Makarov, 2005; Makarov, 1977; Sadybasov, 1990*]. East-west dimensions of such basins and of the ranges between them, however, are only ~100–

300 km (Figures 1, 2, and 3). Accordingly, despite the linearity of the belt as a whole, along-strike variations within it make finding a typical cross section difficult [e.g., *Laverov and Makarov, 2005; Makarov, 1977; Sadybasov, 1990*]. Moreover, the deep structure of the belt, as reflected in both crustal thickness [e.g., *Kosarev et al., 1993; Oreshin et al., 2002; Vinnik et al., 2002*] and upper mantle structure [e.g., *Li et al., 2009; Roecker et al., 1993; Wolfe and Vernon, 1998*], shows marked differences both across and along the strike of the range.

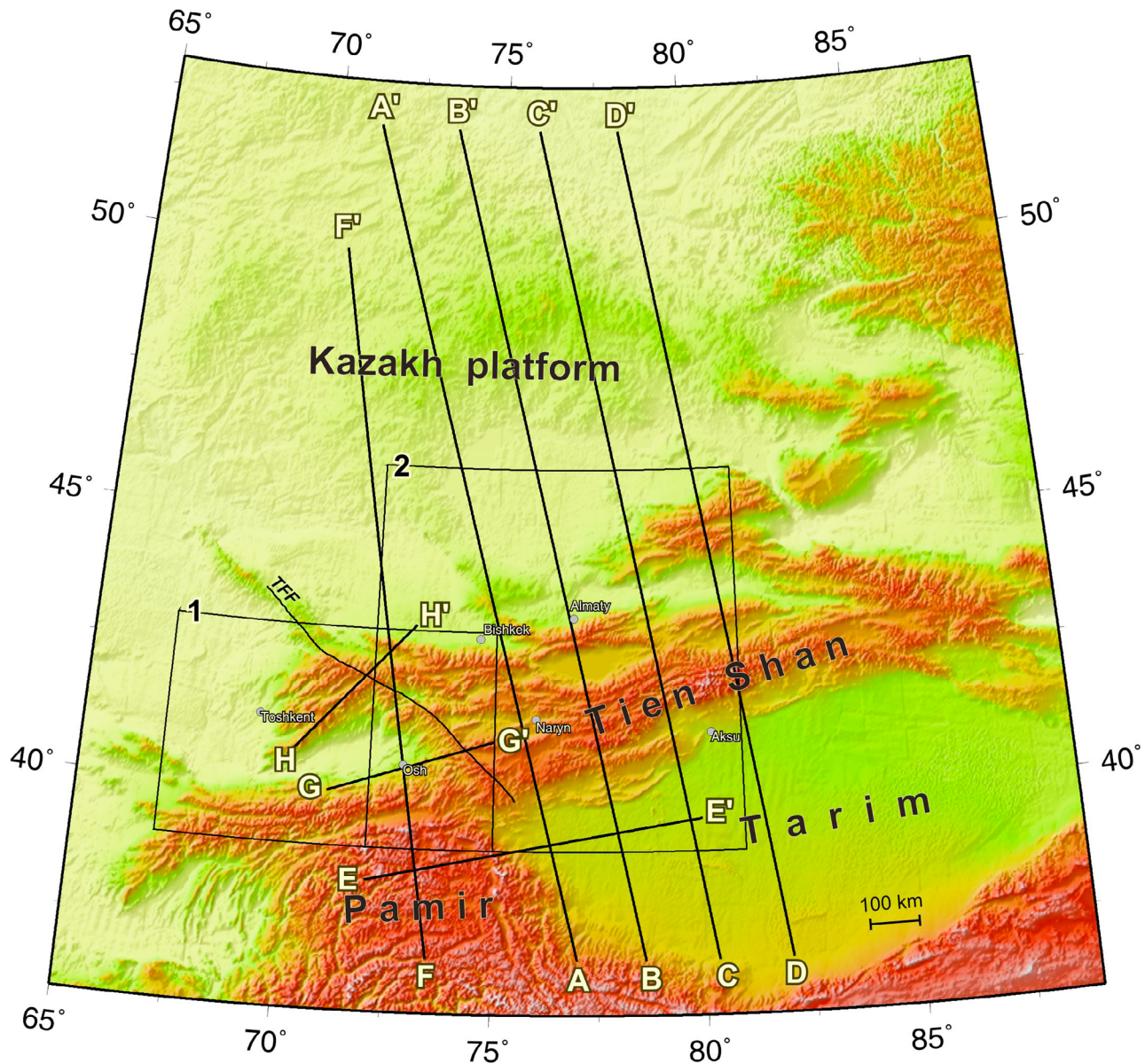


**Figure 2.** Map of region with GPS points and showing names of key localities, lines of profiles in Figures 4, 5, 7, and 9, and regions where smaller maps are shown. The region labeled 1 is shown in Figure 6, and that labeled 2 is in Figure 8.

[5] To the south of the Tien Shan, the Tarim Basin (Figures 1–3) appears to deform sufficiently slowly that its movement relative to Eurasia has been described as a rigid body rotation about an axis just south of the southeastern edge of the basin [e.g., *Calais et al.*, 2006; *England and Molnar*, 2005; *Kuzikov and Mukhamediev*, 2010; *Meade*, 2007; *Reigber et al.*, 2001; *Shen et al.*, 2001; *Thatcher*, 2007]. In most such treatments, root-mean-square (RMS) differences in relative velocities among points in the basin are less than 2 mm/yr, and as small as 1 mm/yr for some studies.

[6] At the western end of the Tien Shan, the Ferghana Valley (Figures 1–3) also seems to undergo only mild de-

formation except on its edges [e.g., *Reigber et al.*, 2001; *Thomas et al.*, 1993; *Ulomov*, 1974]. Mountain ranges to the north of the Ferghana Valley, including the Chatkal Range, and to its south, the South Tien Shan, absorb relative movement of the basin with respect to the regions on its flanks. Seismicity on the edge of the valley is relatively high, but only sparse small earthquakes have been located beneath its center (Figure 1). Sediment has accumulated within the valley since at least Mesozoic time, and high terrain seems to have surrounded the region for much of that time [e.g., *Kreydenkov and Raspopin*, 1972; *Kuzichkina*, 1972; *Sinityn*, 1960, pp. 101–109; *Sinityn*, 1962]. Paleomagnetic declination anomalies suggest as much as 20°–30° of counterclockwise rotation of the basin and the neigh-

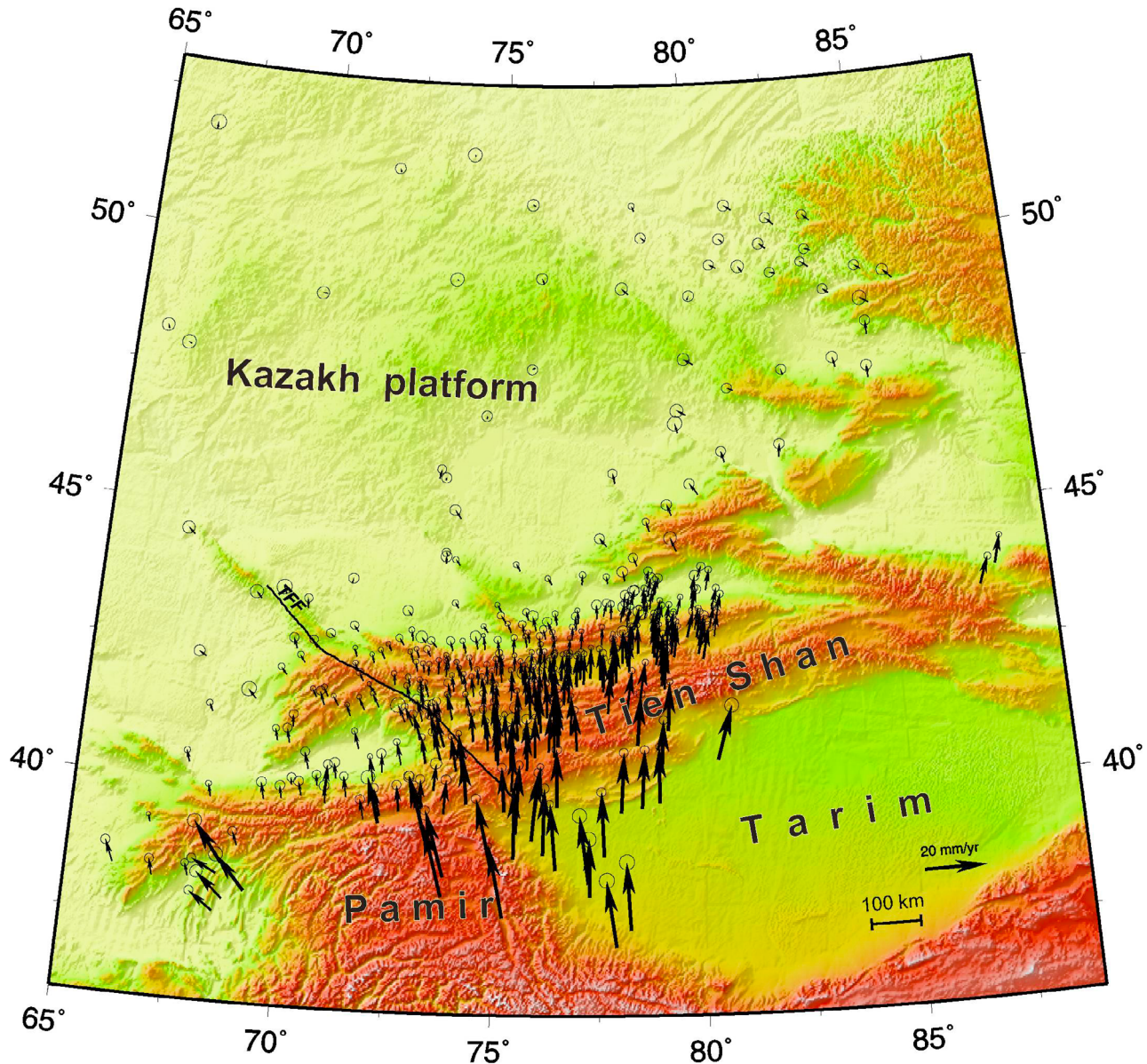


**Figure 3.** Map of region with GPS velocities, relative to Eurasia. Error ellipses show 95% confidence ellipses.

boring Chatkal Range with respect to Eurasia [Bazhenov, 1993; Thomas *et al.*, 1993]. Thus, the Ferghana Valley seems to have maintained its identity as a block since Mesozoic time.

[7] To the west of the Tarim Basin and south of the South Tien Shan, the Pamir shares features that typify the Tibetan Plateau: a high, relatively flat plateau (Figures 2 and 3), where normal faulting and east-west extension appear to dominate active deformation [e.g., Burtman and Molnar, 1993; Strecker *et al.*, 1995]. Many of the same east-west trending sutures and fragments of Gondwana that had been accreted to Eurasia during Phanerozoic time can be identified in the Pamir and in the Hindu Kush of Afghanistan farther west, and it follows that the regions have undergone a similar geologic history, at least perhaps until the Pamir

was displaced northward with respect to most of Tibet, presumably in Cenozoic time [e.g., Burtman and Molnar, 1993; Schwab *et al.*, 2004]. Both the Pamir and Hindu Kush are associated with intermediate-depth seismicity, whose form suggests the presence of a deformed, subducted lithospheric slab at depth [e.g., Mellors *et al.*, 1995; Pavlis and Das, 2000; Roecker, 1982; Vinnik *et al.*, 1977]. The inclined zone of seismicity projects to the surface at northern edge of the Pamir, where concentrated shortening occurs along the Pamir frontal thrust zone, suggesting subduction of continental lithosphere beneath the Pamir [Burtman and Molnar, 1993; Hamburger *et al.*, 1992; Strecker *et al.*, 2003].

[8] We present observations of present-day surface motions within and around the Tien Shan based on 16 years of

geodetic measurements from a dense, regional GPS network (Figures 2 and 3). These data provide quantitative constraints on deformation rates within and around the Tien Shan and in turn within this type area of intracontinental mountain building. A few points for which we can obtain GPS velocities lie within the Pamir, and they allow us to address deformation on its eastern and northern edges.

## 2. GPS Network and Processing

[9] We report results from campaign measurements beginning in 1994 and from a growing number of continuously recording stations in the region since before 1994. In fact, the GPS network that we analyze began as three separate networks each of which grew over time (we give a summary of the history of these networks in the auxiliary material).<sup>1</sup> Table 1 summarizes not only velocities and uncertainties of GPS points, but also dates of the first campaigns used in our determination of the velocity field, durations spanned by remeasurements, and numbers of remeasurement campaigns for each site. Table 1 updates results for subsets of these data analyzed earlier [Abdrakhmatov *et al.*, 1996; Bogomolov *et al.*, 2007; Bragin *et al.*, 2001; Herring *et al.*, 2002; Kuzikov and Mukhamediev, 2010; Laverov and Makarov, 2005; Meade and Hager, 2001; Reigber *et al.*, 2001; Yang *et al.*, 2008; Zubovich *et al.*, 2007].

[10] We processed the GPS observations using the GAMIT/GLOBK software suite [Herring, 2004; King and Bock, 2004], and we estimated uncertainties following standard procedures described by Reilinger *et al.* [2006]. Appendix A gives some details of the processing.

## 3. Results

[11] To present the velocity field we rely on both maps (Figures 3, 6, and 8) and profiles (Figures 4, 5, 7, and 9). We orient profiles perpendicular to the main structures, and plot separately components of velocity parallel and perpendicular to the structures, which allows convergent or divergent and strike-slip components to be separated.

### 3.1. Convergence Between the Tarim Basin and Eurasia

[12] Perhaps the most definitive result is the demonstration that the Tarim Basin moves toward the Kazakh Platform, and hence toward the Eurasian plate, at  $20 (\pm 2)$  mm/yr. Earlier, Abdrakhmatov *et al.* [1996] had inferred such a rate by extrapolating measurements within the Kyrgyz and Kazakh side of the Tien Shan to the Tarim Basin in China. With GPS data from the Tarim Basin, Reigber *et al.* [2001] reported a rate of  $19 \pm 3$  mm/yr for a station in the western Tarim Basin with respect to Eurasia. With more sites in both Tarim and especially within the stable Kazakh Platform, with more measurements at individual sites, and with a time interval spanned by initial and most recent measurements roughly twice that used by Reigber *et al.* [2001], we can refine the rate, as shown most clearly on profiles A-A' and

B-B' (Figures 2 and 4). The lower rates shown for profiles C-C' and D-D' (Figures 2 and 4) derive in part from the southernmost points on these profiles lying within the deforming southern margin of the Tien Shan. Hence the velocities of these points with respect to Eurasia underestimate the convergence rate between Tarim and Eurasia.

[13] As noted above, GPS data from the entire Tarim Basin, including a large area east of where we have data, show that relative to Eurasia Tarim rotates about an axis just south of the eastern end of the basin [e.g., Calais *et al.*, 2006; England and Molnar, 2005; Kuzikov and Mukhamediev, 2010; Meade, 2007; Reigber *et al.*, 2001; Shen *et al.*, 2001; Thatcher, 2007]. Thus, these angular velocities require an eastward decrease of convergence rates of points in Tarim relative to Eurasia, as is apparent also for data along profile E-E' (Figures 2 and 5, blue and green points). These data, from the western part of Tarim, alone are inadequate to improve estimates of angular velocities of Tarim relative to Eurasia, but note that the eastward decrease in rates also contributes to the smaller maximum rates on profiles C-C' and D-D' than on profiles A-A' and B-B' (Figure 4).

[14] At the longitude of the Kyrgyz, or central, Tien Shan ( $\sim 75^\circ\text{E}$ – $80^\circ\text{E}$ ), global GPS data show that India converges with Eurasia at  $\sim 33$  mm/yr [Argus *et al.*, 2010]. Thus, in this segment, shortening across the Tien Shan, by convergence between the Tarim Basin and the Kazakh Platform, absorbs nearly two thirds of India's penetration into Eurasia. Although India seems to underthrust southwestern Tibet at  $\sim 20$  mm/yr [e.g., Jade *et al.*, 2004], the orientation of the Himalaya at this longitude is not perpendicular to the orientation of plate convergence. Thus underthrusting beneath the western Himalaya absorbs only  $\sim 12$ – $13$  mm/yr of India's convergence with Eurasia at this longitude.

[15] Estimated amounts of Cenozoic shortening across the central Tien Shan do not permit shortening at an average rate of  $\sim 20$  mm/yr for more than  $\sim 10$  Myr, and hence suggest a much shorter duration than India has been penetrating into Eurasia (since  $\sim 45$ – $55$  Ma [e.g., Garzanti and Van Haver, 1988; Zhu *et al.*, 2005]). For instance, assuming Airy isostasy and a Cenozoic age of present-day elevations, Avouac *et al.* [1993] inferred as much as  $\sim 220$  km of shortening. With present-day knowledge of crustal thickness, however, this amount seems excessive. Using receiver functions from numerous seismograph stations, Oreshin *et al.* [2002] and Vinnik *et al.* [2002] reported crustal thicknesses of 55–65 km beneath much of the central Tien Shan, compared with  $\sim 45$  km not only beneath the Kazakh Platform to the north and the Tarim Basin to the south, but also beneath the Naryn Basin within the Tien Shan. Makarov *et al.* [2010] inferred similar crustal thicknesses from seismic reflection profiling. Even if one allowed for 20 km of excess crustal thickness beneath a region as wide as 200 km, if that thickening were due to shortening of crust 45 km thick, it would call for only  $\sim 90$  km of shortening. From mapping of structures, Abdrakhmatov *et al.* [2001], inferred as little as 35–80 km of shortening across central Tien Shan in Kyrgyzstan, which constitutes roughly two thirds of the width of the belt. Similarly, both Chedia [1986] and Makarov [1995] [see also Laverov and Makarov, 2005] calculated that 50 km

<sup>1</sup>Auxiliary materials are available in the HTML. doi:10.1029/2010TC002772.

**Table 1.** Coordinates, Velocities, Dates of Installations, and Durations of GPS Recording at Sites<sup>a</sup>

Name	Longitude (°N)	Latitude (°E)	VxI	VyI	VxE	VyE	Sx	Sy	Cor	SYear	Dur	n
AAC4	73.755	42.168	28.3	6.9	-0.1	5.0	0.3	0.3	0.004	1995.6	11.1	6
ABD4	72.050	41.784	26.0	5.7	-2.4	3.1	0.3	0.3	0.010	1995.5	12.0	7
ADA4	75.525	44.132	27.0	3.7	-1.2	2.3	0.4	0.4	0.000	1997.4	9.2	7
ADRA	70.023	40.800	26.9	8.9	-1.0	4.6	0.6	0.6	0.008	1994.7	4.0	3
AIB4	79.969	42.896	29.8	8.5	1.4	8.3	0.4	0.4	0.003	1998.8	7.8	8
AKB4	76.956	42.073	29.1	10.9	0.7	9.7	0.3	0.3	0.006	1995.6	10.8	8
AKBA	73.821	38.503	22.4	24.6	-6.1	21.3	0.6	0.6	0.004	1994.7	4.0	4
AKD4	80.135	47.882	24.9	2.1	-3.0	1.8	0.8	0.7	0.030	2000.6	4.0	5
AKH4	78.542	41.795	30.2	12.5	1.8	11.7	0.4	0.4	-0.005	1998.8	8.0	5
AKJ4	72.145	41.557	26.2	6.9	-2.2	4.3	0.3	0.3	0.011	1995.5	12.0	8
AKK4	76.854	42.885	28.5	5.3	0.1	4.1	0.4	0.4	0.004	1995.6	10.1	7
AKQI	78.451	40.942	29.8	17.3	1.2	16.5	0.6	0.6	0.006	1998.9	4.3	4
AKS4	75.967	40.717	28.3	14.7	-0.2	13.3	0.3	0.3	0.008	1995.8	10.8	10
AKT4	79.851	43.427	29.7	6.8	1.3	6.6	0.5	0.5	0.002	1998.8	6.8	6
AKTA	78.966	39.877	28.8	18.7	0.1	18.2	0.5	0.5	0.006	1998.9	6.3	7
AKTO	75.899	39.196	30.6	23.6	2.1	22.0	0.6	0.6	0.000	1998.9	4.3	3
ALA4	71.460	41.362	26.9	6.2	-1.4	3.5	0.3	0.3	0.007	1995.5	12.0	8
ALB5	76.167	42.313	28.6	7.4	0.1	6.1	0.4	0.4	0.013	1995.8	10.7	6
ALD4	72.258	39.421	21.2	15.2	-7.3	12.7	0.6	0.6	0.035	1999.6	4.8	4
ALM1	69.730	40.829	27.2	7.3	-0.9	3.7	0.5	0.5	-0.027	1994.7	8.1	3
ALT4	77.763	43.908	28.0	3.2	-0.4	2.4	0.4	0.4	0.003	1997.8	7.8	6
ALUN	74.244	40.331	26.5	16.5	-1.7	14.1	0.4	0.4	0.006	1994.7	7.8	7
ANA4	77.603	42.790	28.6	6.7	0.1	5.7	0.3	0.3	0.014	1995.8	10.7	8
AND4	69.514	39.737	27.2	8.6	-1.2	5.4	0.7	0.6	0.060	1999.6	4.8	4
ANGR	70.082	41.102	27.5	8.1	-0.2	3.9	0.6	0.6	0.003	1994.7	4.0	3
ARA4	77.750	41.860	29.5	11.9	1.0	10.9	0.4	0.4	-0.004	1998.8	8.0	5
ARC4	76.665	41.693	28.8	11.2	0.3	10.1	0.7	0.7	0.020	2002.6	3.8	3
ARG4	79.657	46.649	27.3	3.2	-0.8	2.9	0.9	0.9	0.067	2000.6	3.0	4
ARP4	74.827	40.838	27.8	11.1	-0.7	9.4	0.4	0.4	0.008	1997.7	8.9	7
ARS4	72.982	41.244	25.6	8.1	-2.7	6.0	0.4	0.5	0.012	1997.7	6.8	8
ARTU <sup>b</sup>	58.561	56.430	24.6	7.2	-0.9	1.2	0.4	0.4	0.000	1999.6	7.9	33
ASK4	73.538	40.075	29.2	10.8	0.7	8.7	0.7	0.7	0.058	1999.6	4.8	4
ASP4	73.494	42.700	26.4	4.2	-1.9	2.0	0.5	0.5	0.017	1995.6	5.9	4
ASR4	81.105	50.091	26.5	0.8	-1.1	1.0	0.7	0.7	0.027	2000.6	4.0	5
ASS4	78.148	43.310	28.8	5.1	0.5	4.4	0.5	0.5	0.002	1998.8	6.8	6
AST4	76.966	43.059	27.8	5.7	-0.3	4.6	0.5	0.5	0.009	1997.8	7.8	5
ATAI	73.933	41.383	26.8	12.6	-1.1	9.3	0.6	0.6	0.002	1994.7	4.0	3
AWAT	80.393	40.643	33.4	17.3	5.0	17.2	0.9	0.9	0.026	1998.9	2.7	3
AZO4	77.114	43.897	28.5	4.2	0.2	3.2	0.4	0.5	0.003	1997.8	7.8	6
BAB4	73.268	39.513	25.8	13.5	-2.7	11.3	0.6	0.6	0.028	1999.6	4.8	4
BACH	78.540	39.777	29.7	19.7	1.1	18.9	0.6	0.6	0.009	1998.9	4.3	3
BALH	73.980	45.069	26.7	3.8	-1.9	2.7	0.7	0.8	0.011	1995.7	3.0	3
BAN2 <sup>b</sup>	77.512	13.034	46.2	34.6	19.8	33.4	0.6	0.6	0.002	2003.6	3.9	16
BAR4	77.616	42.008	28.7	12.0	0.1	11.0	0.5	0.5	0.036	1998.8	6.9	5
BAU4	75.019	41.576	28.0	7.8	-0.4	6.2	0.4	0.4	0.003	1997.7	8.9	9
BAY4	75.083	41.079	27.4	11.1	-1.1	9.5	0.4	0.4	0.007	1997.7	8.9	8
BAYS	67.046	38.175	26.5	10.3	-1.2	5.1	0.6	0.6	0.017	1994.7	4.0	3
BER4	75.657	42.957	27.7	5.1	-0.6	3.6	0.5	0.5	0.014	1995.6	6.0	4
BES4	75.795	42.818	27.9	4.9	-0.5	3.5	0.3	0.3	0.006	1995.6	11.1	6
BESH	70.524	40.357	26.5	9.5	-1.4	5.3	0.6	0.6	0.008	1994.7	4.0	3
BET4	75.030	40.646	28.2	12.1	-0.2	10.4	0.4	0.4	0.005	1997.7	8.9	8
BIN4	79.416	45.137	26.9	3.9	-1.4	3.6	0.7	0.7	0.036	2000.6	4.0	5
BKE4	75.426	40.757	28.1	13.3	-0.4	11.9	0.7	0.7	0.020	2002.6	4.0	4
BOK4	73.212	42.768	27.0	4.0	-1.3	1.8	0.8	0.7	-0.001	1995.6	3.8	3
BOL4	83.984	49.038	25.9	0.6	-1.7	1.3	0.7	0.7	0.007	2000.6	4.0	5
BOR4	73.235	41.648	27.1	7.6	-1.2	5.4	0.4	0.4	0.011	1995.6	8.8	6
BOST	71.283	43.777	28.4	4.9	0.3	1.8	0.7	0.7	0.004	1995.7	3.0	3
BOZ4	71.792	41.495	26.2	6.6	-2.0	3.9	0.3	0.3	0.010	1995.5	12.0	8
BRL4	70.520	42.569	26.8	5.3	-1.2	2.5	0.6	0.6	0.018	1997.4	5.1	5
BTK4	70.765	40.048	27.9	6.5	-0.6	3.6	0.6	0.6	0.033	1999.6	4.8	4
BTR4	75.020	41.186	27.2	11.4	-1.1	9.7	0.4	0.4	0.004	1997.7	8.9	9
BULU	74.951	38.662	23.6	24.5	-5.1	22.7	0.6	0.6	-0.004	1998.9	4.3	4
BUR4	79.053	42.261	29.8	11.7	1.4	11.1	0.4	0.4	-0.001	1998.8	8.0	6
BUZ4	76.432	42.811	27.6	5.0	-0.8	3.7	0.3	0.4	0.003	1995.6	10.1	7
BYS4	75.729	42.749	27.8	5.0	-0.5	3.4	0.3	0.3	0.004	1995.6	11.1	5
CAR1	68.104	41.245	26.4	6.7	-1.3	2.5	0.4	0.4	0.020	1994.7	7.8	7
CATK	71.721	42.014	25.5	8.8	-2.2	4.9	0.6	0.6	0.003	1994.7	4.0	3
CAUV	72.090	40.199	26.9	10.8	-1.4	7.8	0.4	0.4	0.006	1994.7	9.8	7

Table 1. (continued)

Name	Longitude (°N)	Latitude (°E)	VxI	VyI	VxE	VyE	Sx	Sy	Cor	SYear	Dur	n
CEK4	75.750	40.686	28.6	14.3	0.1	12.9	0.7	0.7	0.021	2002.6	4.0	4
CHA4	71.721	42.015	27.0	5.2	-1.4	2.7	0.5	0.5	0.019	1995.5	6.2	5
CHIL	78.878	43.584	29.0	8.4	1.1	6.4	0.6	0.6	0.006	1994.7	4.0	3
CHK4	77.739	41.527	29.3	13.7	0.9	12.7	0.6	0.6	0.007	1998.8	4.9	4
CHL4	77.845	43.267	28.3	5.7	0.0	4.8	0.4	0.5	0.002	1997.8	7.8	5
CHLK	78.373	43.529	28.9	4.8	0.5	4.4	0.7	0.7	0.005	2004.4	2.1	4
CHO4	77.075	42.719	28.6	6.8	0.3	5.7	0.3	0.3	0.018	1995.8	10.7	8
CHR4	78.976	43.271	29.6	6.3	1.2	5.7	0.4	0.4	0.001	1997.8	8.8	10
CHT4	76.052	41.334	28.2	13.2	-0.4	11.9	0.7	0.7	0.019	2002.6	4.0	5
CHU4	74.002	43.423	27.2	3.6	-1.1	1.8	0.4	0.4	-0.005	1997.4	8.2	5
CHUM <sup>b</sup>	74.751	42.999	26.9	3.8	-1.4	2.0	0.3	0.3	0.003	1997.7	9.8	35
CHY4	72.875	41.966	27.6	5.2	-0.7	2.9	0.4	0.4	0.005	1995.5	9.3	7
DAL4	78.457	43.137	29.5	6.5	1.2	5.8	0.4	0.4	0.000	1997.8	8.8	10
DANG	69.200	38.043	17.8	16.5	-9.6	10.9	0.9	0.9	0.022	1994.7	2.0	3
DAR4	75.041	40.782	28.0	12.1	-0.5	10.4	0.4	0.4	0.005	1997.7	8.9	8
DAT4	72.286	39.573	26.4	11.2	-2.1	8.7	0.6	0.6	0.031	1999.6	4.8	4
DEGE	75.766	43.245	27.4	4.1	-0.8	2.6	0.5	0.5	0.012	1995.5	7.0	7
DENA	67.880	38.235	26.6	8.0	-1.1	3.8	0.5	0.4	0.016	1994.7	8.1	4
DJA4	76.498	41.245	28.1	14.4	-0.4	13.2	0.7	0.7	0.012	2002.6	4.0	4
DJAN	66.106	38.338	24.6	12.0	-2.9	6.7	0.6	0.6	0.020	1994.7	4.0	3
DJE4	73.956	41.896	27.7	7.2	-0.8	5.3	0.3	0.3	0.005	1995.6	11.1	6
DJR4	74.469	40.987	27.7	10.9	-0.9	9.2	0.5	0.5	0.006	2000.5	6.1	5
DNG4	73.619	40.925	25.5	11.2	-2.9	9.4	0.6	0.6	0.008	2000.5	4.3	4
DOR4	79.877	43.380	29.8	7.4	1.5	7.0	0.6	0.7	0.028	1998.8	4.8	4
DRB4	69.128	41.552	25.6	6.2	-2.6	2.8	0.9	0.8	0.071	1999.5	3.0	4
DSO4	78.668	43.432	29.0	5.7	0.7	5.1	0.4	0.4	0.004	1998.8	7.8	10
DUSC	68.625	38.516	22.6	15.4	-9.4	12.7	0.9	0.9	0.026	1994.7	2.0	3
DYU4	74.366	41.476	26.8	8.5	-1.6	6.7	0.4	0.4	0.000	1997.7	9.1	8
EGA4	76.367	43.005	26.6	5.0	-1.7	3.7	0.6	0.6	0.020	1995.6	4.1	3
EKS4	76.742	42.070	28.9	10.4	0.5	9.2	0.3	0.3	0.008	1995.6	10.8	9
ELB4	76.468	41.820	28.0	10.8	-0.5	9.5	0.3	0.3	0.006	1995.6	11.1	7
ELG4	74.215	42.618	27.3	5.6	-1.0	3.7	0.3	0.3	0.007	1995.6	9.8	6
ELS4	75.051	42.624	27.8	5.9	-0.6	4.2	0.5	0.5	0.007	1995.6	6.1	4
EME4	74.452	41.821	27.5	8.2	-0.9	6.3	0.3	0.3	0.005	1995.6	11.1	6
ENG4	76.422	41.494	29.0	13.8	0.3	12.6	0.7	0.7	0.025	2002.6	3.8	3
ESE4	80.308	43.061	30.1	7.5	1.6	7.3	0.4	0.4	0.001	1998.8	7.8	8
GAK4	84.931	48.221	27.6	3.1	-0.1	4.4	0.7	0.7	0.019	2000.6	4.0	5
GARA	68.515	37.642	20.3	10.4	-7.9	5.8	0.6	0.6	0.012	1994.7	4.0	3
GAZE	75.479	38.853	28.8	24.7	0.1	23.2	0.5	0.5	-0.002	1998.9	6.3	7
GBL4	78.787	43.664	29.0	6.8	0.8	6.1	0.7	0.7	0.014	1998.8	3.7	4
GKO4	76.725	42.171	28.5	9.2	0.1	8.1	0.4	0.4	0.009	1999.5	7.0	6
GKU4	78.921	43.039	29.4	6.7	1.1	6.2	0.4	0.4	0.003	1998.8	7.8	9
GSO4	78.621	43.546	29.2	5.7	0.8	4.9	0.4	0.4	0.005	1998.8	7.8	7
GTA4	77.139	42.071	28.8	10.9	0.3	9.7	0.4	0.4	0.009	1998.8	7.7	7
GUAO <sup>b</sup>	87.177	43.471	31.2	6.9	3.3	8.5	0.5	0.5	0.002	2002.5	5.0	18
HEB4	83.590	49.828	25.5	0.0	-2.0	0.7	0.7	0.7	0.004	2000.6	4.0	5
HOK4	76.767	42.641	28.8	6.1	0.6	4.8	0.3	0.3	0.010	1995.6	10.8	7
HON4	73.802	42.426	27.6	4.4	-0.8	2.4	0.3	0.3	-0.006	1995.6	11.1	4
HRT4	73.067	42.493	27.4	5.0	-0.9	2.8	0.3	0.3	0.008	1995.6	11.8	5
HYDE <sup>b</sup>	78.551	17.417	42.3	34.0	14.9	33.1	0.6	0.5	0.001	2003.6	3.9	16
IISC <sup>b</sup>	77.570	13.021	43.2	35.8	16.3	34.8	0.3	0.3	-0.001	1995.5	12.0	47
IKZ4	73.796	39.654	29.0	13.2	0.7	11.0	0.7	0.6	0.003	1999.6	4.8	4
ILI4	78.188	43.953	27.6	3.9	-0.6	3.1	0.7	0.7	0.023	1998.8	3.7	3
INY4	79.070	42.015	30.2	12.2	1.9	11.6	0.3	0.3	0.003	1995.8	10.9	7
IRKT <sup>b</sup>	104.316	52.219	25.2	-5.5	-0.8	0.6	0.3	0.3	-0.004	1995.8	11.7	43
ISH4	78.210	41.601	30.1	13.2	1.7	12.4	0.4	0.5	-0.002	1998.8	8.0	5
ISY5	77.490	43.261	28.1	5.6	-0.2	4.7	0.6	0.8	0.038	1997.8	5.7	4
JAM4	71.526	42.908	26.8	4.8	-1.5	2.0	0.6	0.5	0.013	1997.4	5.1	5
JANG	70.804	41.533	26.3	8.4	-1.6	4.4	0.6	0.6	0.003	1994.7	4.0	4
JAP4	78.681	43.254	29.5	5.6	1.0	5.0	0.4	0.4	0.003	1998.8	7.8	14
JET4	78.274	42.297	28.5	11.6	0.1	10.8	0.4	0.4	0.003	1995.8	7.9	6
JIAS	76.734	39.497	26.6	20.8	-2.1	19.3	0.6	0.6	-0.013	1998.9	4.3	4
JJO4	75.334	43.011	27.2	4.3	-1.1	2.8	0.4	0.4	0.000	1995.6	11.0	6
JLK4	73.686	40.637	25.5	11.0	-2.8	8.9	0.5	0.5	0.004	1997.7	4.8	7
JNI4	78.224	43.104	28.8	5.7	0.5	5.0	0.4	0.5	0.004	1998.8	6.8	6
JUA4	75.645	42.105	27.5	8.2	-0.8	6.6	0.3	0.3	0.014	1995.5	11.1	9
K031	61.594	51.835	27.3	5.8	0.6	0.8	0.9	0.7	-0.011	1998.6	4.0	3
K051	66.316	51.751	27.0	6.2	0.1	2.4	1.0	0.7	0.019	1998.6	4.0	3



Table 1. (continued)

Name	Longitude (°N)	Latitude (°E)	VxI	VyI	VxE	VyE	Sx	Sy	Cor	SYear	Dur	n
K071	65.795	48.052	27.0	5.2	-0.5	1.2	0.8	0.7	0.037	1998.6	4.0	3
K081	70.019	49.013	26.1	3.1	-1.5	0.2	0.8	0.7	0.017	1998.6	4.0	3
K091	66.462	47.828	26.6	4.3	-1.0	0.5	0.9	0.7	0.042	1998.6	4.0	3
K100	67.176	44.401	25.8	5.7	-2.2	2.1	0.8	0.8	0.022	1998.6	3.9	3
K111	69.034	43.376	26.3	5.2	-1.8	2.1	0.9	0.8	0.025	1998.6	2.9	3
K121	69.650	43.504	27.2	5.1	-0.9	2.1	1.0	0.8	0.040	1998.6	2.9	3
K131	70.285	53.126	26.8	3.7	-0.2	1.1	0.8	0.6	0.041	1998.6	4.0	3
K141	74.010	51.694	27.0	2.2	-0.3	0.4	0.9	0.7	0.025	1998.6	4.0	3
K151	71.848	51.338	27.0	3.4	-0.3	1.1	0.7	0.7	0.018	1998.6	4.0	3
K161	73.660	49.407	27.2	2.4	-0.4	0.5	0.9	0.7	0.055	1998.6	4.0	3
K171	74.571	46.908	28.1	2.5	0.1	0.9	0.7	0.7	0.025	1998.6	4.0	3
K181	73.553	45.755	28.2	2.8	0.2	0.9	0.7	0.7	0.018	1998.6	4.0	3
K191	75.783	50.808	26.7	1.7	-0.7	0.5	0.8	0.7	0.021	1998.6	4.0	3
K201	78.900	50.168	26.3	1.4	-1.3	1.0	0.7	0.7	0.042	1998.6	4.0	3
K211	78.406	49.194	25.7	2.5	-2.0	1.9	0.8	0.8	0.058	1998.6	4.0	3
K221	76.064	49.385	26.9	3.0	-0.7	1.8	0.7	0.7	0.028	1998.6	4.0	3
K231	75.844	47.852	27.0	0.8	-0.8	-0.5	0.7	0.7	0.020	1998.6	4.0	3
K241	80.047	49.065	28.2	1.3	0.5	1.3	0.7	0.7	0.025	1998.6	4.0	3
KAB4	81.609	49.528	26.3	1.7	-1.1	1.9	0.8	0.7	0.019	2000.6	4.0	5
KAI4	76.101	41.173	27.5	14.1	-0.8	12.5	0.5	0.5	0.024	1995.8	6.9	7
KAK1	72.904	42.806	27.4	6.2	-0.6	3.2	0.4	0.4	0.008	1994.7	7.8	10
KAL4	76.397	42.306	29.0	7.2	0.5	5.9	0.4	0.4	0.008	1999.5	7.0	4
KALA	78.037	39.714	29.6	20.1	1.0	19.2	0.6	0.6	0.010	1998.9	4.3	4
KALP	79.035	40.503	29.4	16.4	0.8	15.6	0.6	0.6	0.007	1998.9	4.3	3
KAR4	76.776	41.733	28.6	12.2	0.2	10.9	0.4	0.4	0.019	1995.8	10.7	6
KARA	70.963	39.959	28.3	12.6	0.3	8.6	0.6	0.6	0.004	1994.7	4.0	3
KARL	73.460	38.957	21.8	27.4	-6.7	24.1	0.6	0.6	0.007	1994.7	4.0	3
KAS4	75.443	42.300	28.3	6.5	-0.1	5.1	0.3	0.3	0.006	1995.6	11.1	6
KAST	75.967	43.045	27.2	5.8	-1.2	4.8	0.7	0.8	0.005	2004.4	2.1	4
KASU	76.840	41.132	28.4	14.4	0.1	12.8	0.3	0.3	0.005	1994.7	11.9	8
KAT4	80.008	42.740	30.2	10.0	1.9	9.8	0.7	0.6	0.017	1998.8	4.8	5
KAZA <sup>b</sup>	73.944	41.385	26.4	10.0	-2.0	8.0	0.3	0.3	0.002	1997.7	9.8	33
KAZY	69.824	42.036	26.3	5.6	-1.9	2.3	0.4	0.4	0.017	1995.5	7.0	8
KBU4	71.579	42.202	27.1	4.9	-1.1	2.3	0.3	0.4	0.008	1995.5	12.0	6
KEK4	76.057	42.759	28.3	4.7	-0.1	3.3	0.5	0.5	0.014	1995.8	6.0	4
KELI	77.906	37.258	25.7	22.2	-3.0	21.3	1.0	0.8	0.021	1998.9	2.7	4
KEN4	72.367	42.593	27.2	4.7	-1.0	2.2	0.3	0.3	0.011	1995.5	12.0	7
KET4	80.355	43.400	30.2	6.9	1.8	6.9	0.5	0.5	0.005	1998.8	6.8	6
KFIR	67.868	37.838	10.5	8.1	-17.6	3.3	0.6	0.6	0.014	1994.7	4.0	3
KHA4	73.672	44.380	27.8	3.1	-0.4	1.2	0.5	0.6	0.005	1997.4	5.1	4
KHZ4	72.297	40.362	28.0	8.6	-0.5	6.1	0.6	0.6	0.038	1999.6	4.8	4
KIN4	74.066	42.204	27.6	6.1	-0.8	4.2	0.3	0.3	0.002	1995.6	11.1	6
KIT3 <sup>b</sup>	66.885	39.135	27.6	6.1	-0.7	2.2	0.3	0.3	0.000	1995.5	12.0	44
KIZI	76.463	38.656	27.1	22.8	-1.7	21.4	0.5	0.5	0.002	1998.9	6.3	7
KJA6	73.190	41.001	25.8	10.0	-2.7	8.0	0.5	0.5	-0.015	1997.7	7.1	5
KKA4	72.894	41.695	27.0	7.2	-1.3	4.9	0.4	0.4	0.014	1995.5	8.9	7
KKB4	72.735	39.678	27.6	10.8	-1.0	8.3	0.6	0.6	0.025	1999.6	4.8	4
KKC4	74.928	41.737	28.1	7.9	-0.5	6.3	0.4	0.4	0.001	1997.7	9.1	8
KKD4	76.205	41.902	27.9	10.7	-0.5	9.3	0.5	0.5	0.023	1995.8	6.9	5
KKO4	75.146	42.257	27.8	6.8	-0.6	5.2	0.4	0.4	0.010	1995.5	10.1	7
KKT4	70.222	43.271	27.1	5.4	-1.1	2.4	0.6	0.6	0.009	1997.4	5.1	5
KKY4	75.550	41.018	27.5	12.3	-1.0	10.9	0.8	0.7	0.029	1998.8	3.9	4
KLM4	70.975	39.742	27.8	8.6	-0.7	5.7	0.6	0.6	0.028	1999.6	4.8	4
KNG4	71.464	39.875	27.4	9.4	-1.1	6.7	0.6	0.6	0.031	1999.6	4.8	4
KNS4	78.825	43.024	29.5	6.7	1.1	6.0	0.4	0.4	0.001	1997.8	8.8	9
KOG4	76.408	41.892	27.2	11.1	-1.3	9.9	0.7	0.7	0.024	2002.6	3.8	3
KOK4	78.646	43.452	29.1	5.3	0.7	4.7	0.4	0.4	0.003	1997.8	8.8	12
KOL4	79.885	46.959	24.9	1.8	-2.8	1.6	0.8	0.8	0.035	2000.6	3.0	4
KOR4	84.959	49.412	25.3	0.4	-2.0	1.4	0.7	0.7	0.013	2000.6	4.0	5
KOS4	76.520	40.918	28.5	15.3	-0.1	14.0	0.7	0.7	0.010	2002.6	4.0	4
KOVK	73.881	41.808	27.4	6.3	-1.1	4.4	0.5	0.5	0.015	1999.8	5.8	3
KOY4	79.092	42.166	30.1	11.8	1.8	11.4	0.3	0.3	0.010	1995.8	10.9	7
KRB4	76.072	41.781	28.3	10.4	-0.2	8.9	0.3	0.3	0.004	1995.6	11.1	7
KRC4	85.066	48.797	25.1	0.7	-2.6	1.7	0.9	0.9	0.049	2000.6	3.0	4
KRK4	71.904	39.494	27.1	8.9	-1.4	6.3	0.6	0.6	0.048	1999.6	4.8	4
KRL6	76.434	41.122	27.9	14.0	-0.6	12.5	0.4	0.4	0.008	1995.8	10.8	6
KRM4	78.161	43.483	28.7	4.7	0.4	4.0	0.6	0.6	0.014	1997.8	4.7	4

Table 1. (continued)

Name	Longitude (°N)	Latitude (°E)	VxI	VyI	VxE	VyE	Sx	Sy	Cor	SYear	Dur	n
KRS4	79.926	43.027	29.7	7.4	1.4	7.1	0.4	0.4	0.005	1998.8	7.8	9
KRT4	75.048	41.487	27.8	9.0	-0.7	7.4	0.4	0.4	0.005	1997.7	8.9	8
KRTV <sup>b</sup>	78.619	50.714	26.6	2.4	-0.8	1.7	0.4	0.4	0.003	2000.7	6.7	19
KRU4	76.443	40.734	28.5	14.7	-0.1	13.3	0.7	0.7	0.012	2002.6	4.0	4
KRV4	73.667	41.344	27.0	8.3	-1.6	6.4	0.5	0.5	0.000	2000.5	6.1	4
KSH4	77.744	44.592	25.9	3.5	-2.2	2.7	0.6	0.7	0.026	2000.6	4.0	5
KSHI <sup>b</sup>	75.923	39.517	31.0	19.8	2.4	18.3	0.4	0.4	0.003	1998.9	6.3	5
KST4	83.998	47.670	27.0	2.6	-0.8	3.3	0.7	0.7	0.022	2000.6	4.0	5
KSTU <sup>b</sup>	92.794	55.993	24.8	-3.1	-1.4	0.3	0.4	0.4	0.002	1997.7	7.1	28
KTA4	70.940	42.783	26.8	3.8	-1.4	1.1	0.6	0.6	0.005	1997.4	4.3	4
KTAU	70.940	42.783	26.2	4.5	-2.1	1.7	0.7	0.6	0.082	1995.5	7.0	5
KTE4	76.387	42.619	28.8	6.2	0.4	4.9	0.4	0.4	0.022	1995.6	10.8	4
KTSS	73.385	45.785	28.0	6.4	0.6	3.0	0.6	0.6	0.001	1994.7	4.0	3
KTY4	76.198	42.895	27.6	4.5	-0.8	3.1	0.5	0.5	0.011	1995.6	6.1	5
KUD4	79.858	43.630	29.7	7.3	1.4	7.1	0.7	0.7	0.020	1998.8	3.7	4
KUK4	75.761	41.749	28.8	9.1	0.5	7.6	0.8	0.8	0.050	2002.6	3.8	3
KUL4	76.298	40.816	28.8	14.3	0.4	13.0	0.3	0.3	0.010	1995.8	10.8	9
KUM4	70.601	41.669	26.8	5.5	-1.4	2.5	0.3	0.3	0.007	1995.5	12.0	8
KUN4	75.569	41.358	27.6	11.8	-0.8	10.2	0.3	0.3	0.012	1995.8	10.7	9
KUR4	75.086	43.379	26.9	3.8	-1.4	2.3	0.3	0.4	0.000	1995.5	11.1	7
KURA	72.832	43.253	26.9	4.4	-1.2	1.7	0.7	0.7	0.003	1995.7	3.0	3
KURG	68.715	37.874	18.9	11.9	-8.8	7.9	0.8	0.8	0.016	1994.7	4.0	3
KURY	76.339	43.894	27.8	3.1	-0.6	2.2	0.8	0.8	0.008	2004.4	2.1	4
KUT4	76.339	43.894	26.9	3.2	-1.2	2.0	0.4	0.4	-0.001	1997.4	9.2	7
KYZ4	75.135	42.092	27.7	7.5	-0.7	5.8	0.3	0.3	0.006	1995.5	11.2	8
KYZY	73.323	39.379	23.1	19.1	-5.0	16.4	0.7	0.7	0.015	1995.7	3.0	3
KZY4	75.977	40.523	29.6	13.9	1.1	12.5	0.7	0.7	0.019	2002.6	4.0	4
KZZ4	78.314	43.522	29.8	5.6	1.7	4.7	0.7	0.7	0.014	1998.8	3.7	5
LAM4	69.933	39.774	27.8	7.2	-0.8	4.1	0.6	0.6	0.057	1999.6	4.8	4
LEDI	68.526	38.323	20.2	8.9	-8.0	4.1	0.6	0.6	0.012	1994.7	4.0	3
LHAS <sup>b</sup>	91.104	29.657	46.1	16.8	17.4	19.4	0.3	0.3	0.000	1995.5	11.2	46
LHAZ <sup>b</sup>	91.104	29.657	46.3	17.2	17.5	19.7	0.5	0.5	-0.002	2002.5	5.0	17
LJM4	73.221	41.572	27.3	8.1	-1.1	5.9	0.4	0.4	0.012	1996.7	7.7	6
MARK	77.624	38.904	27.9	22.1	-0.8	20.9	0.6	0.6	0.016	1998.9	4.3	4
MAT4	78.501	44.225	27.4	3.4	-1.1	2.8	0.6	0.6	0.015	2000.6	5.0	6
MAY1	76.478	43.155	27.5	5.5	-0.6	3.7	0.4	0.4	0.007	1994.7	8.0	10
MDG4	70.157	40.035	28.1	5.4	-0.3	2.4	0.6	0.6	0.033	1999.6	4.8	4
MER4	73.341	42.524	26.9	4.5	-1.1	2.3	0.5	0.5	0.010	1995.6	6.8	5
MKR4	73.045	42.248	27.7	5.2	-0.6	3.0	0.4	0.4	0.009	1995.6	9.9	5
MNJ4	79.323	42.757	29.2	10.5	0.8	10.1	0.5	0.5	0.001	1998.8	5.8	6
MOL4	75.038	41.669	27.8	8.4	-0.7	6.7	0.3	0.3	0.004	1995.5	11.2	8
MUD4	76.572	41.129	27.3	14.0	-1.2	12.7	0.9	0.9	0.047	2002.6	2.9	3
MUJI	74.427	39.024	22.7	20.7	-5.9	19.0	0.5	0.4	0.000	1998.9	6.3	7
MUN4	78.112	42.439	28.5	10.8	0.1	10.0	0.4	0.4	-0.004	1998.8	8.0	7
MURG	73.796	38.137	22.1	26.5	-6.2	23.1	0.6	0.6	0.005	1994.7	4.0	4
MUS4	73.318	42.175	28.4	5.8	0.1	3.6	0.4	0.4	0.007	1995.6	9.9	6
NAR5	76.255	41.446	28.2	12.5	-0.3	11.0	0.4	0.4	0.016	1995.8	10.7	8
NBA4	80.000	42.599	30.8	10.8	2.4	10.5	0.7	0.7	0.012	1998.8	3.7	4
NGS4	75.730	41.875	27.5	8.6	-0.9	7.1	0.8	0.8	0.003	2002.6	3.8	3
NJK4	77.946	42.248	28.1	11.9	-0.4	11.1	0.4	0.4	-0.004	1998.8	8.0	6
NJT4	78.238	42.406	27.0	11.7	-1.3	10.9	0.8	0.8	0.012	1998.8	2.7	4
NKR4	79.210	42.665	29.3	11.0	0.9	10.3	0.4	0.4	0.004	1998.8	8.0	6
NKU4	78.284	43.013	32.6	6.3	4.2	5.6	0.7	0.7	0.023	1998.8	3.9	5
NRIL <sup>b</sup>	88.360	69.362	21.6	-1.0	-1.4	1.2	0.4	0.4	0.000	2001.3	6.2	26
NRK4	74.690	41.820	27.8	8.2	-0.7	6.5	0.4	0.4	-0.001	1997.7	9.1	8
NSB4	73.763	40.880	25.6	11.3	-2.9	9.2	0.4	0.4	-0.003	1997.7	7.1	7
NTE4	79.210	43.139	29.5	7.1	1.1	6.6	0.4	0.4	0.004	1998.8	7.8	8
NTP4	78.374	42.684	28.4	8.4	-0.1	7.5	0.4	0.4	0.002	1998.8	8.0	7
NVSK <sup>b</sup>	83.235	54.841	26.2	0.5	-0.6	1.0	0.4	0.4	0.007	2000.6	6.8	24
OBO4	75.849	41.433	27.7	12.8	-0.8	11.4	0.7	0.7	0.025	2002.6	3.8	4
OGI4	74.549	42.040	28.0	6.8	-0.5	5.0	0.3	0.3	0.005	1995.6	11.1	5
OKI4	73.933	41.383	27.1	9.5	-1.4	7.5	0.3	0.3	0.005	1995.6	11.0	8
OKT1	67.670	40.291	27.0	7.8	-1.1	3.6	0.4	0.4	0.003	1994.7	8.1	4
ONA4	75.983	41.577	27.8	10.4	-0.8	9.1	0.8	0.8	0.035	2002.6	3.8	4
ORGO	77.918	42.440	28.0	10.5	-0.5	9.6	0.3	0.3	0.003	1995.5	11.2	6
OSH4	72.743	40.522	26.8	9.6	-1.6	7.3	0.4	0.5	0.013	1997.7	6.8	8
OTM4	73.201	42.235	27.8	5.0	-0.4	2.7	0.3	0.3	0.011	1995.5	12.0	8

Table 1. (continued)

Name	Longitude (°N)	Latitude (°E)	VxI	VyI	VxE	VyE	Sx	Sy	Cor	SYear	Dur	n
OTTU	75.827	41.655	24.8	12.2	-3.2	9.5	0.6	0.6	0.010	1994.7	4.0	3
OYT4	74.076	40.436	26.6	13.2	-1.9	11.3	0.4	0.4	-0.004	1997.7	7.1	8
PAK4	75.130	40.848	27.6	11.9	-0.9	10.3	0.4	0.4	0.004	1997.7	8.9	8
PAN0	80.040	43.994	29.5	3.9	1.3	3.5	0.5	0.5	0.020	1995.5	5.0	10
PCH4	79.060	42.396	29.3	10.8	0.9	10.3	0.4	0.4	-0.003	1998.8	8.0	6
PDB4	80.228	43.756	29.5	6.8	1.2	6.6	0.4	0.5	0.006	1998.8	6.8	6
PISH	78.246	37.559	27.6	22.6	-1.2	21.9	1.0	0.8	0.009	1998.9	2.7	3
PKZ4	78.076	43.208	29.2	5.7	0.9	4.9	0.7	0.7	0.017	1998.8	3.9	4
PODG <sup>b</sup>	79.485	43.328	29.6	6.0	1.3	5.6	0.3	0.3	0.002	1998.6	8.9	28
POL2 <sup>b</sup>	74.694	42.680	27.7	6.3	-0.6	4.5	0.3	0.3	-0.001	1995.5	12.0	48
PPR4	78.292	42.547	28.8	9.8	0.4	9.0	0.4	0.4	0.000	1998.8	8.0	7
PSE4	82.598	50.357	24.9	1.9	-2.5	2.4	0.7	0.7	0.010	2000.6	4.0	5
PSH4	78.926	42.721	28.7	10.1	0.3	9.4	0.4	0.4	0.004	1998.8	8.0	7
PTO4	78.861	42.620	29.3	9.7	0.9	9.1	0.4	0.4	0.001	1998.8	8.0	6
PTU4	75.088	40.578	28.2	12.3	-0.4	10.8	0.4	0.4	0.007	1997.7	8.9	8
PUR4	73.627	41.288	25.8	8.8	-2.5	6.8	0.4	0.4	0.000	1997.7	7.1	7
QIAK	75.404	40.094	29.1	14.6	0.6	13.1	0.5	0.5	0.017	1998.9	6.3	7
QIQI	76.978	40.844	28.0	14.1	-0.7	13.2	0.5	0.5	0.015	1998.9	6.3	6
RAL4	74.252	41.912	27.5	7.4	-0.9	5.5	0.3	0.3	0.007	1995.6	11.1	6
RAS4	82.306	46.121	28.3	4.0	0.4	4.2	0.7	0.7	0.039	2000.6	4.0	5
RGA4	75.195	43.174	26.7	4.3	-1.6	2.6	0.5	0.5	0.014	1995.6	6.8	4
RKA4	79.142	41.964	29.0	13.0	0.5	12.5	0.8	0.8	0.008	1998.8	2.7	4
RKR4	74.742	41.726	27.7	7.8	-0.8	6.2	0.4	0.4	0.001	1997.7	9.1	7
RKT4	79.066	42.121	29.1	11.2	0.7	10.7	0.4	0.4	-0.005	1998.8	8.0	6
RSO4	75.370	41.760	28.7	8.2	0.0	6.7	0.3	0.3	0.004	1995.5	11.2	9
RSR4	75.732	41.697	28.2	9.3	-0.2	7.8	0.3	0.3	0.004	1995.8	10.9	9
RTC4	70.391	39.864	27.4	7.2	-1.1	4.3	0.6	0.6	0.042	1999.6	4.8	4
RTR4	72.667	42.706	27.0	4.6	-1.4	2.3	0.5	0.5	0.007	1995.6	6.8	5
RTS4	78.906	42.548	28.7	10.9	0.3	10.4	0.4	0.4	-0.002	1998.8	8.0	7
RYB4	76.103	42.523	29.6	7.2	1.1	5.6	0.4	0.4	0.013	1995.8	6.0	4
SAAZ	79.740	42.905	29.9	10.1	2.0	8.4	0.6	0.6	0.009	1994.7	4.0	3
SAK4	76.715	42.250	29.5	8.0	1.1	6.8	0.4	0.4	0.005	1995.1	7.0	6
SAL4	82.550	49.471	25.7	0.0	-1.8	0.4	0.7	0.7	0.014	2000.6	4.0	5
SAN1	68.246	39.694	27.1	8.1	-1.0	4.1	0.4	0.4	0.002	1994.7	8.1	4
SAN4	70.881	41.697	26.8	5.7	-1.5	2.8	0.4	0.4	0.016	1995.5	8.9	7
SAR4	85.794	49.193	24.7	1.7	-2.8	2.9	0.7	0.7	0.011	2000.6	4.0	5
SARY	71.701	40.774	26.5	8.7	-1.7	5.6	0.4	0.4	0.003	1994.7	8.1	3
SAS4	78.972	42.751	29.3	7.7	0.9	7.1	0.3	0.3	0.008	1995.8	10.9	8
SAST	70.024	42.526	26.3	7.5	-1.2	3.3	0.6	0.6	0.001	1994.7	4.0	3
SATY	78.408	43.057	30.0	6.4	1.5	6.0	0.7	0.7	0.004	2004.4	2.1	4
SAUK	72.248	39.439	23.7	19.6	-3.8	14.4	0.9	0.9	0.019	1994.7	2.0	3
SBA4	80.117	42.503	30.3	10.6	2.0	10.3	0.7	0.7	0.004	1998.8	3.7	4
SDT4	81.186	47.381	25.9	0.8	-1.9	0.8	0.7	0.7	0.036	2000.6	4.0	5
SDY4	74.153	42.052	27.4	6.8	-1.1	5.0	0.3	0.3	0.004	1995.6	11.1	6
SELE <sup>b</sup>	77.017	43.179	28.0	5.5	-0.3	4.4	0.3	0.3	0.002	1997.4	10.1	42
SEM4	76.045	42.275	28.4	8.1	0.0	6.8	0.3	0.3	0.008	1995.6	10.8	7
SEX4	78.742	43.900	29.0	4.8	0.7	4.2	0.5	0.6	0.017	1998.8	4.8	5
SGD4	78.813	43.430	29.2	6.2	0.8	5.7	0.4	0.5	0.007	1998.8	6.8	9
SHA5	75.397	42.622	28.5	6.9	0.2	5.1	0.4	0.4	0.067	1995.5	9.9	4
SHAC	77.248	38.412	25.7	22.6	-2.7	21.9	0.9	0.9	0.015	1998.9	2.7	3
SHB4	72.080	39.861	30.3	10.4	1.8	7.8	0.9	0.9	0.061	1999.6	4.8	4
SHD4	80.487	43.251	29.7	7.7	1.4	7.5	0.5	0.5	0.015	1998.8	6.8	4
SHE4	78.936	43.690	29.4	6.0	1.2	5.5	0.6	0.6	0.018	1997.8	4.7	4
SHI4	71.532	42.454	27.3	5.3	-0.9	2.7	0.3	0.3	0.010	1995.5	12.0	7
SHL4	79.304	42.868	29.7	7.0	1.3	6.5	0.4	0.4	0.006	1998.8	7.8	8
SHY5	72.789	41.302	25.8	7.9	-2.4	5.4	1.0	1.0	0.036	2001.7	2.8	3
SJK4	77.959	42.095	28.6	12.1	0.1	11.2	0.4	0.4	-0.002	1998.8	8.0	6
SKA4	72.920	42.410	27.2	5.6	-1.0	3.3	0.3	0.3	0.013	1995.5	12.0	7
SKR4	79.322	42.604	30.3	10.9	1.8	10.4	0.4	0.4	0.002	1998.8	8.0	6
SKT4	76.354	42.246	29.2	8.2	0.8	6.6	0.4	0.5	0.011	1999.5	7.0	6
SLP4	83.491	49.541	25.0	1.0	-2.5	1.9	0.6	0.6	0.008	2000.6	4.0	5
SME4	75.772	40.476	28.7	13.9	0.2	12.4	0.6	0.6	0.015	2002.6	4.0	4
SMO4	77.627	41.918	28.9	12.0	0.4	11.0	0.4	0.4	-0.002	1998.8	8.0	6
SON4	75.423	41.914	27.5	8.6	-1.0	7.1	0.3	0.3	0.003	1995.5	11.2	9
SOS4	73.901	42.644	27.4	5.1	-0.9	3.1	0.5	0.6	0.014	1995.6	5.9	3
SRB4	78.307	42.786	28.6	7.1	0.2	6.3	0.3	0.3	0.007	1995.8	10.9	8
SRT4	78.275	43.227	29.0	5.6	0.7	4.8	0.5	0.5	0.004	1998.8	6.8	5

Table 1. (continued)

Name	Longitude (°N)	Latitude (°E)	VxI	VyI	VxE	VyE	Sx	Sy	Cor	SYear	Dur	n
SSR4	77.890	42.349	28.3	10.7	-0.3	9.7	0.4	0.4	-0.001	1998.8	8.0	7
STE4	75.814	42.128	28.7	7.4	0.3	6.0	0.8	0.8	0.017	2002.6	3.8	3
SUG4	78.226	43.433	29.2	5.0	0.9	4.3	0.6	0.6	0.020	1998.8	4.8	5
SUGU	76.512	39.806	28.3	20.2	-0.2	18.7	0.6	0.6	-0.016	1998.9	4.3	4
SUM4	80.412	42.906	29.6	7.8	1.1	7.7	0.4	0.4	0.008	1998.8	7.8	8
SUMK <sup>b</sup>	73.997	44.208	26.8	3.8	-1.3	1.9	0.4	0.4	0.002	2000.7	6.7	22
SUU4	73.555	42.206	28.4	6.6	0.1	4.5	0.4	0.4	0.007	1995.5	9.9	7
SYT4	73.257	39.732	28.0	11.8	-0.5	9.6	0.6	0.6	0.023	1999.6	4.8	4
TAKR	67.809	42.233	25.3	5.7	-2.4	1.4	0.7	0.7	0.006	1995.7	3.0	3
TALA <sup>b</sup>	72.210	42.446	27.0	5.2	-1.2	2.7	0.3	0.3	0.003	1998.8	8.7	32
TALD	73.657	44.238	27.8	5.0	-0.1	2.3	0.7	0.8	0.009	1995.7	3.0	3
TAM4	77.553	42.137	28.4	11.3	-0.1	10.2	0.4	0.4	0.005	1998.8	7.7	7
TASH <sup>b</sup>	75.234	37.775	24.0	24.9	-4.6	23.2	0.4	0.4	0.003	1998.9	6.3	6
TEG4	76.594	42.137	28.8	9.7	0.4	8.4	0.3	0.3	0.012	1995.8	10.7	7
TEK4	78.842	44.855	27.2	3.7	-1.0	3.3	0.5	0.5	0.005	1997.8	6.8	6
TEM4	73.333	41.785	27.0	6.6	-1.3	4.4	0.4	0.4	0.011	1995.6	8.8	5
TEN4	80.866	46.081	27.0	3.6	-1.0	3.5	0.6	0.7	0.032	2000.6	4.0	5
TER4	71.146	41.539	26.5	5.7	-1.8	3.0	0.3	0.3	0.011	1995.5	12.0	8
TGU4	74.722	41.511	27.5	8.2	-0.8	6.5	0.4	0.4	0.006	1997.7	8.9	8
THR4	75.263	40.889	27.8	12.3	-0.7	10.8	0.4	0.4	0.006	1997.7	8.9	8
TOK6	75.837	42.355	28.7	6.7	0.3	5.2	0.3	0.3	0.008	1995.5	11.0	8
TON4	77.052	42.157	29.0	10.1	0.5	8.8	0.4	0.4	0.004	1998.8	7.7	7
TOR4	73.160	41.895	27.6	5.7	-0.7	3.5	0.4	0.4	0.013	1995.5	8.9	7
TOS4	77.311	42.176	28.6	10.9	0.3	9.9	0.3	0.3	0.011	1995.8	10.7	9
TRG4	75.383	40.578	28.3	13.4	-0.2	11.9	0.4	0.4	0.006	1997.7	8.9	9
TRM4	83.630	50.382	25.1	1.3	-2.2	2.0	0.6	0.7	0.005	2000.6	4.0	5
TRY4	80.126	45.514	25.5	3.7	-2.6	3.5	0.7	0.7	0.032	2000.6	4.0	5
TSH5	74.790	42.055	27.9	7.9	-0.5	6.2	0.4	0.4	-0.007	1997.7	9.1	4
TUA4	78.948	42.415	29.2	11.5	0.8	10.9	0.3	0.3	0.007	1995.8	10.9	8
TUM4	79.297	43.029	29.9	6.5	1.4	6.1	0.4	0.4	0.007	1998.8	7.8	8
TUR4	77.642	43.315	29.4	5.3	1.1	4.4	0.5	0.6	0.006	1997.8	5.7	4
TURG	75.388	40.517	28.3	14.0	-0.2	12.6	0.5	0.5	0.006	1998.9	6.3	7
TUS4	73.824	42.320	27.8	4.9	-0.5	2.9	0.3	0.3	0.005	1995.5	11.2	7
TUT4	71.203	40.212	27.6	7.8	-0.8	5.0	0.7	0.6	0.045	1999.6	4.8	4
TYUP	78.509	42.632	28.3	9.6	-0.1	9.0	0.3	0.3	0.003	1995.5	11.2	9
TZB4	73.334	40.569	27.0	10.4	-1.5	8.3	0.5	0.5	0.017	1997.7	6.8	8
UGAM	70.254	42.280	26.5	5.5	-1.7	2.4	0.4	0.4	0.015	1995.5	7.0	8
UKO4	75.959	41.934	27.8	9.3	-0.7	7.9	0.3	0.3	0.005	1995.6	11.1	7
ULT4	78.926	42.858	28.9	7.9	0.4	7.5	0.4	0.4	0.004	1998.8	7.8	8
ULU4	75.080	42.346	28.0	6.6	-0.4	4.9	0.5	0.5	0.016	1995.6	6.0	4
ULUG	74.336	39.842	27.1	17.7	-1.4	15.6	0.6	0.6	0.004	1998.9	4.3	4
URD1	75.086	43.379	27.4	6.6	-0.3	3.4	0.7	0.7	0.005	1994.7	4.0	7
URM4	71.958	42.354	27.4	5.2	-0.8	2.7	0.3	0.3	0.013	1995.5	12.0	7
URS4	76.338	42.110	28.1	8.8	-0.4	7.6	0.4	0.4	0.001	1995.6	10.1	7
URUM <sup>b</sup>	87.601	43.808	30.4	7.0	2.4	8.9	0.4	0.3	0.003	1998.9	8.6	33
USH4	77.969	45.739	27.3	4.2	-0.7	3.3	0.6	0.6	0.013	2000.6	4.0	5
UUM4	73.478	41.219	26.5	9.9	-2.0	7.9	0.4	0.4	0.001	1997.7	7.1	7
UYG4	79.532	44.478	26.4	4.9	-1.9	4.4	0.8	0.9	0.042	2000.6	3.0	4
UZB4	74.929	41.936	27.8	8.0	-0.6	6.2	0.3	0.3	0.004	1995.6	11.1	6
UZG4	74.780	41.069	27.3	10.7	-1.2	9.1	0.5	0.5	0.008	2000.5	6.1	5
UZL4	79.022	43.144	29.6	6.8	1.2	6.3	0.4	0.5	0.006	1998.8	6.8	8
UZU4	72.498	41.980	27.9	5.9	-0.4	3.6	0.4	0.4	0.004	1995.5	9.3	7
VAV4	81.414	50.667	25.0	1.4	-2.4	1.6	0.7	0.7	0.029	2000.6	4.0	5
VJK4	77.863	42.031	28.6	12.1	0.2	11.2	0.4	0.4	-0.007	1998.8	8.0	6
VKA4	79.392	42.546	29.8	10.3	1.3	9.9	0.4	0.4	0.004	1998.8	8.0	6
VKE4	78.833	42.898	29.4	7.4	1.0	6.8	0.5	0.5	0.001	1998.8	6.8	4
VKR4	76.336	42.185	29.4	8.5	1.1	7.2	0.4	0.4	0.005	1995.5	7.0	6
VSE4	74.999	42.221	28.0	6.9	-0.4	5.2	0.3	0.3	0.007	1995.6	11.1	6
VTG4	76.744	42.040	29.0	10.8	0.6	9.6	0.4	0.4	0.006	1998.8	7.7	6
VTU4	76.981	42.021	28.4	11.2	-0.1	10.0	0.4	0.4	0.004	1998.8	7.7	7
WARZ	68.967	38.854	26.2	9.1	-1.7	4.3	0.6	0.6	0.003	1994.7	4.0	4
WUPA	75.510	39.311	29.8	23.8	1.1	22.2	0.6	0.6	0.002	1998.9	5.2	5
WUQI	75.250	39.718	27.6	16.2	-1.0	14.3	0.6	0.6	0.002	1998.9	4.3	4
WUSH <sup>b</sup>	79.210	41.202	29.3	16.2	0.8	15.7	0.4	0.4	0.002	1998.9	6.3	7
YENG	76.174	38.935	29.0	23.0	0.4	21.4	0.6	0.6	-0.004	1998.9	4.3	3
YUZ4	75.741	41.979	27.8	9.1	-0.6	7.7	0.3	0.3	0.007	1995.6	11.0	8
YZG4	73.207	41.335	26.6	8.9	-1.9	6.9	0.7	0.6	-0.004	2000.5	4.3	4

**Table 1.** (continued)

Name	Longitude (°N)	Latitude (°E)	VxI	VyI	VxE	VyE	Sx	Sy	Cor	SYear	Dur	n
ZAR4	82.322	49.934	25.3	1.2	-2.1	1.6	0.7	0.7	0.016	2000.6	4.0	5
ZAS4	84.856	47.434	27.6	3.1	-0.2	4.0	0.7	0.7	0.034	2000.6	4.0	5
ZBA4	75.009	41.092	27.3	11.1	-1.2	9.4	0.4	0.4	0.006	1997.7	8.9	9
ZEPU	77.277	38.174	27.9	19.4	-0.2	18.4	1.0	0.8	0.004	1998.9	4.3	4
ZES4	80.889	49.619	25.5	1.2	-2.2	1.2	0.7	0.7	0.029	2000.6	4.0	5
ZKK4	74.379	42.302	27.6	5.7	-0.9	4.0	0.4	0.4	0.002	1997.7	9.1	7
ZTR4	82.566	47.611	27.3	1.4	-0.5	1.8	0.7	0.7	0.028	2000.6	4.0	5

<sup>a</sup>VxI and VyI give eastward and northward components of velocity in the ITRF2005 reference frame. VxE and VyE give eastward and northward components of velocity in reference frame tied to Eurasia. Sx and Sy give standard errors in eastward and northward components of velocity, and Cor gives the correlation coefficient between these uncertainties. SYear gives the date when the site was first measured, Dur gives the elapsed time between that first measurement and the most recent measurement campaign, and n gives the number of campaigns during which a site was measured.

<sup>b</sup>Continuously recording site.

of shortening suffices to account for the Cenozoic structure of the Kyrgyz Tien Shan. *Heermance et al.* [2008] offered a minimum bound of 10 to 32 km of shortening on the south side of the range. If between 100 and 200 km of crustal shortening occurred within the Kyrgyz and Chinese Tien Shan, then at the current rate, the entire range would have been built in only 5 to 10 Myr.

[16] The rapid shortening today corroborates other inferences of a recent acceleration of deformation within the Tien Shan long after India collided with Eurasia [e.g., *Abdrakhmatov et al.*, 1996, 2001]. Abrupt increases in sedimentation in basins both within the Tien Shan and on its margins are commonly interpreted as evidence for the emergence of high terrain near or since ~10 Ma [e.g., *Abdrakhmatov et al.*, 2001; *Bullen et al.*, 2001; *Charreau et al.*, 2005, 2006, 2008, 2009; *Ji et al.*, 2008; *Makarov*, 1977; *Shultz*, 1948; *Sun and Zhang*, 2009; *Sun et al.*, 2004, 2009; *Trifonov et al.*, 2008]. Rapid cooling of rock within the Kyrgyz Range beginning near 11 Ma also suggests an abrupt increase in exhumation rates at that time [*Bullen et al.*, 2003; *Sobel and Dumitru*, 1997; *Sobel et al.*, 2006a]. Neither this evidence, however, nor the present-day high convergence rate requires that the Tien Shan formed in late Cenozoic time. Mountain building deformation of the crust of the Tien Shan started near the end of the Oligocene or the beginning of the Miocene Epoch [*Chedia*, 1986; *Makarov*, 1977; *Shultz*, 1948; *Sinitsyn*, 1962]. Similarly, dating of deformation on the south side of the Tien Shan demonstrates active faulting beginning at 20–25 Ma [*Heermance et al.*, 2008; *Yin et al.*, 1998], an inference consistent with both cooling ages near 25 Ma [*Hendrix et al.*, 1994; *Sobel and Dumitru*, 1997; *Sobel et al.*, 2006b] and changes in sedimentation rates in basins flanking the Tien Shan [e.g., *Charreau et al.*, 2009; *Huang et al.*, 2006, 2010; *Ji et al.*, 2008]. Thus, an acceleration of convergence across the Tien Shan beginning at or since ~10 Ma seems to be required, but we cannot distinguish a continuously increasing rate from an abrupt change near or since ~10 Ma and a constant rate since that time.

### 3.2. Deformation Within the Tien Shan

[17] As is clear both on maps of velocities (Figures 3 and 6) and on profiles of components of velocity (Figure 4),

components perpendicular to the Tien Shan show a monotonically decreasing rate across the belt, from Tarim to the southern part of the Kazakh Platform. The velocity gradient is steepest at distances between ~400 and ~700 km for profiles A-A' to D-D' in Figures 2 and 4. In an analysis of active faulting in the area crossed by profile A-A' (Figures 2 and 4a), *Makarov* [1977] [see also *Makarov et al.*, 2010] not only reported active faults on the edge of the Tien Shan, but they also described active faulting within the belt. Later, *Thompson et al.* [2002] and *Abdrakhmatov et al.* [2007] discussed four such faults within the high terrain of the range slipping at ~1 mm/yr or more, and other more minor faults. In a profile of GPS velocities across this region, they showed steep gradients and high strain rates where they had mapped active faults. Moreover, the differences in velocity across these steep gradients matched (with allowance for uncertainties) the slip rates that they had determined for the faults. Our profile A-A' shows a difference of 8–10 mm/yr across the southern margin of the Tien Shan between 300 and 350 km on the profile (Figure 2), where *Scharer et al.* [2004] had inferred a Quaternary rate of ~5 to 7.8 mm/yr, a second difference of 3–4 mm/yr across the Naryn Basin (near 500 km) and near where *Thompson et al.* [2002] had inferred slip at ~4 mm/yr by dating warped terraces and offsets on faults, and hints of smaller differences of 1–2 mm/yr across steep gradients farther north near 600 and 650 km, again near faults that they had mapped. Moreover, as is clearer farther east on profiles C-C' and D-D' (Figures 4c and 4d), GPS points just north of the Kyrgyz Range move northward at 1–2 mm/yr with respect to the Kazakh Platform and Eurasia. Some shortening seems to occur not only within the Dzungarian Alatau (the high terrain between 44.5°N and 45.5°N on the eastern margin of Figure 6) and its westward continuation, but also north of it within the Kazakh Platform (Figures 2–4).

[18] Indications of steep gradients in the velocity field are also present along profile B-B' (Figures 2 and 4b) at three places: (1) a difference of ~5 mm/yr between ~300 and 450 km, north of the southern edge of the Tien Shan and north of or within the fold-and-thrust belt that bounds the belt; (2) another of ~5–6 mm/yr near 600 km, within the Tien Shan between the southern and northern edges of Issyk-Kul and the large basin that it occupies; and (3) a hint

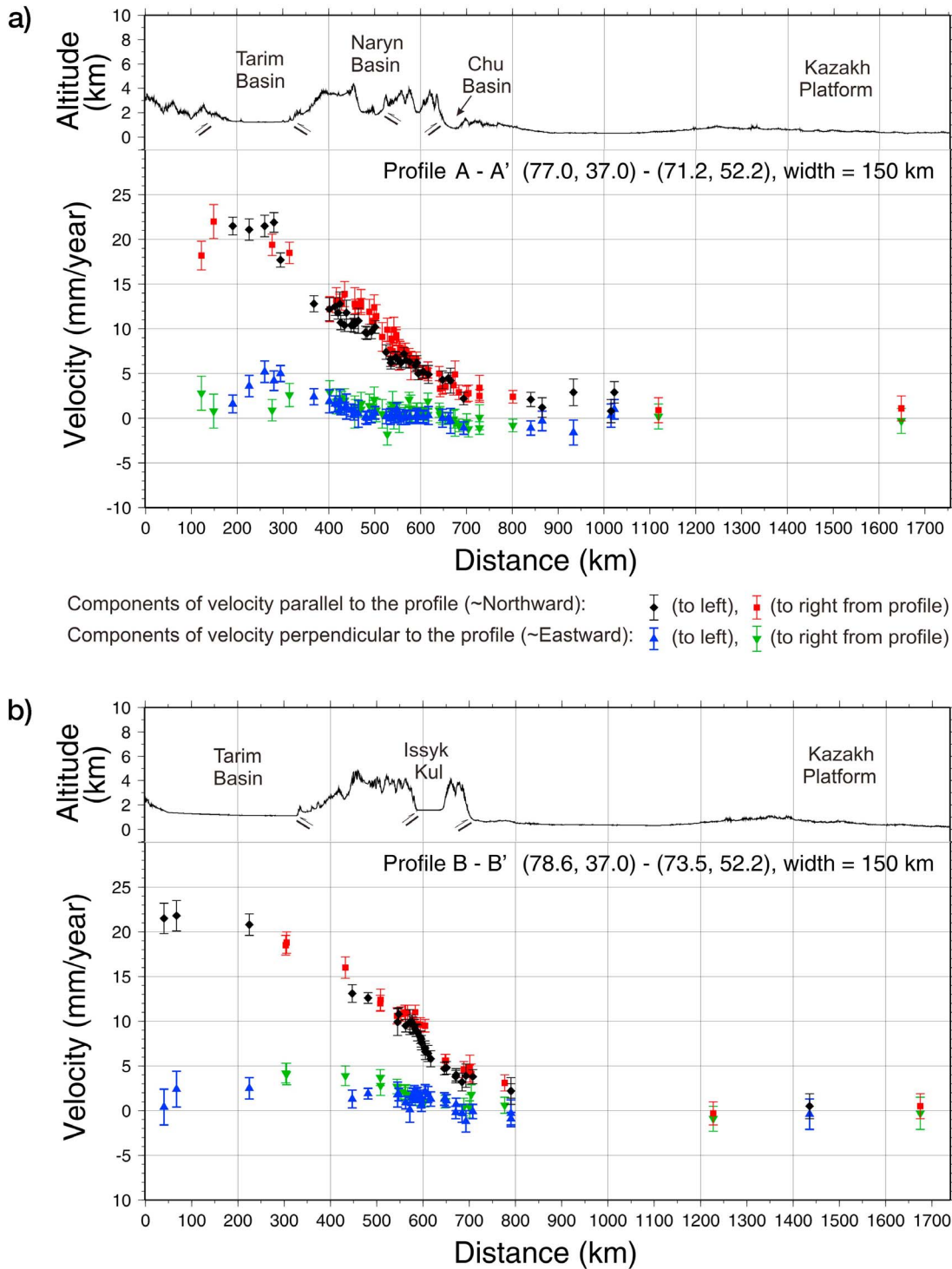


**Figure 4.** (a–d) Profiles of components of velocity across the Tien Shan relative to Eurasia (profiles A–A' to D–D' in Figure 2). As shown in the legend below profile A, components perpendicular to the Tien Shan (and parallel to profiles) are shown with red squares and black diamonds, and components parallel to the Tien Shan (and perpendicular to profiles) are shown with blue and green triangles. Thus, positive values show convergent (approximately northward) components, or movement to the right (approximately eastward). Error bars give  $1\sigma$  uncertainties. Black squares and blue upward pointing triangles show rates of points that lie within 75 km to the west, and red squares and green downward pointing triangles show points within 75 km to the east of the profiles in Figure 2. Thrust fault symbols are shown where active thrust faults have been mapped, as by *Thompson et al.* [2002] for profile A, or inferred from sharp breaks in the topography.

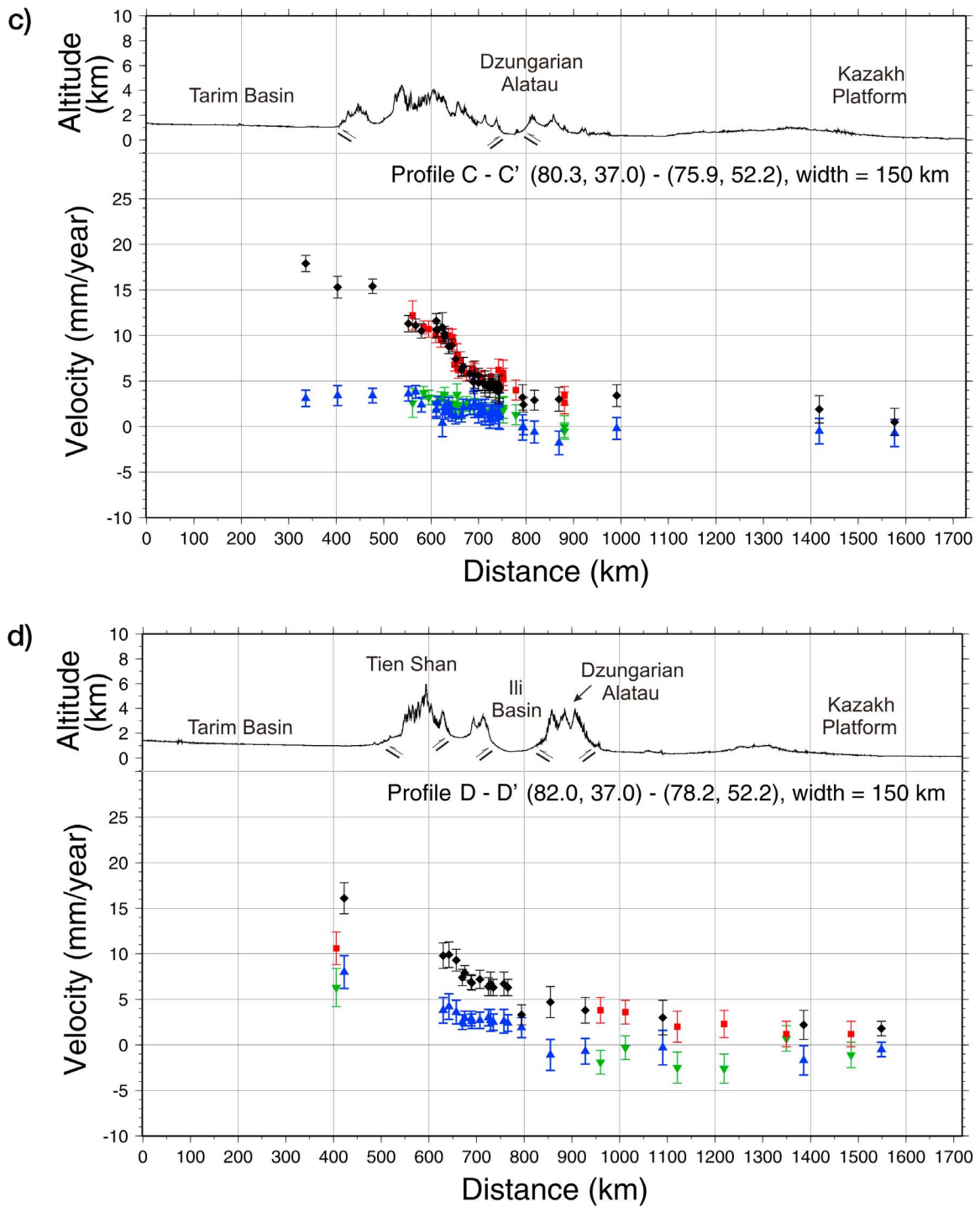
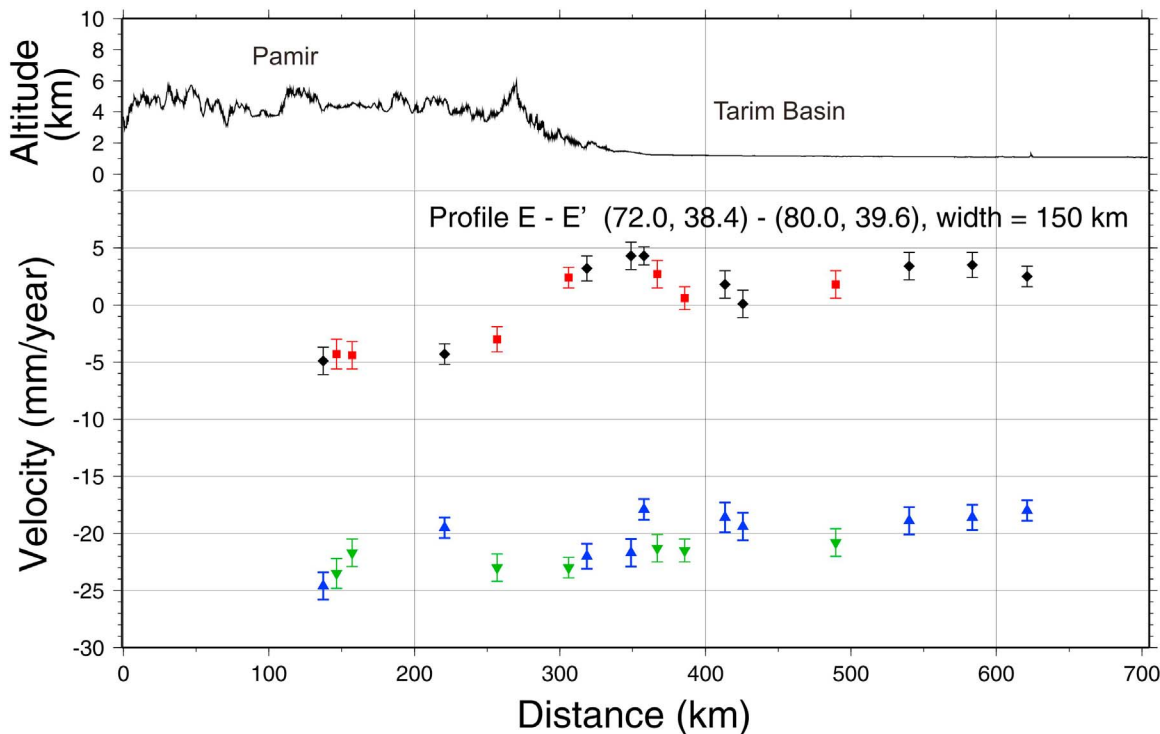


Figure 4. (continued)



Components of velocity parallel to the profile ( $\sim$ Eastward):  $\blacklozenge$  (to left),  $\blacksquare$  (to right from profile)  
 Components of velocity perpendicular to the profile ( $\sim$ Southward):  $\blacktriangleup$  (to left),  $\blacktriangledown$  (to right from profile)

**Figure 5.** Profile of components of velocity across the eastern Pamir into the Tarim Basin relative to Eurasia (profile E-E' in Figure 2). Positive values for black diamonds and red squares indicate approximately eastward components, and the more negative values at points to the west imply divergence along the profile. Positive values for blue upward pointing triangles and green downward pointing triangles indicate movement to the right of the profile and hence approximately southward movement relative to Eurasia. Error bars give  $1\sigma$  uncertainties. Black diamonds and blue upward pointing triangles show rates of points within 75 km to the north of profile E-E' in Figure 2, and red squares and green downward pointing triangles show points within 75 km to the south of it.

of a steep gradient with a difference of  $\sim 2$  mm/yr near 700 km across the northern edge of the Tien Shan, where it bounds the southern edge of the Ili Basin (Figure 6). There is evidence for shortening between the Ili Basin and the Kazakh Platform, with 3–5 mm/yr of shortening across the westward continuation of the Dzungarian Alatau (Figure 6).

[19] Indications of steep gradients suggestive of faults like those inferred by *Thompson et al.* [2002] are present on profile C-C' (Figures 2 and 4c) again in three places: (1) a difference of  $\sim 4$  mm/yr between 500 and 550 km, north of the southern edge of the Tien Shan and north of the fold-and-thrust belt that bounds the belt; (2) another steep gradient with a difference of  $\sim 4$  mm/yr near 650 km, within the Tien Shan, just east of Issyk-Kul and the large basin that it occupies; and (3) the suggestion of steep gradient with a small difference of  $\sim 2$  mm/yr near 750 km across the northern edge of the Tien Shan, where it bounds the southern edge of the Ili Basin (Figures 4c and 6). Points at the western end of the Ili Basin move 2–3 mm/yr with respect to Eurasia.

[20] With only sparse data, steep velocity gradients can be inferred for profile D-D' (Figures 2 and 4d), but they cannot

be defined as well as on profiles A-A', B-B', and C-C'. Several points in the Ili Basin, however, move northward with respect to Eurasia at  $\sim 2$ –3 mm/yr, and that movement is absorbed, at least partly, by shortening across the Dzungarian Alatau.

### 3.3. Strike-Parallel Deformation Within the Tien Shan

[21] Convergence of the Tarim Basin toward the Kazakh Platform is clearly oblique to the strike of the Tien Shan, and accordingly there is a left-lateral strike-slip component of movement parallel to the belt (Figures 3, 4, and 6). Because inferred axes of rotation of the Tarim Basin with respect to Eurasia lie south of the southeastern end of the Tarim Basin [*Calais et al.*, 2006; *England and Molnar*, 2005; *Meade*, 2007; *Reigber et al.*, 2001; *Shen et al.*, 2001; *Thatcher*, 2007] and therefore only 1000–1500 km from the Kyrgyz Tien Shan, directions of relative movement vary measurably over short distances (Figure 6). Points just south of the Tien Shan along profile D-D' move with a left-lateral component of  $\sim 4$  mm/yr with respect to Eurasia, but points farther west



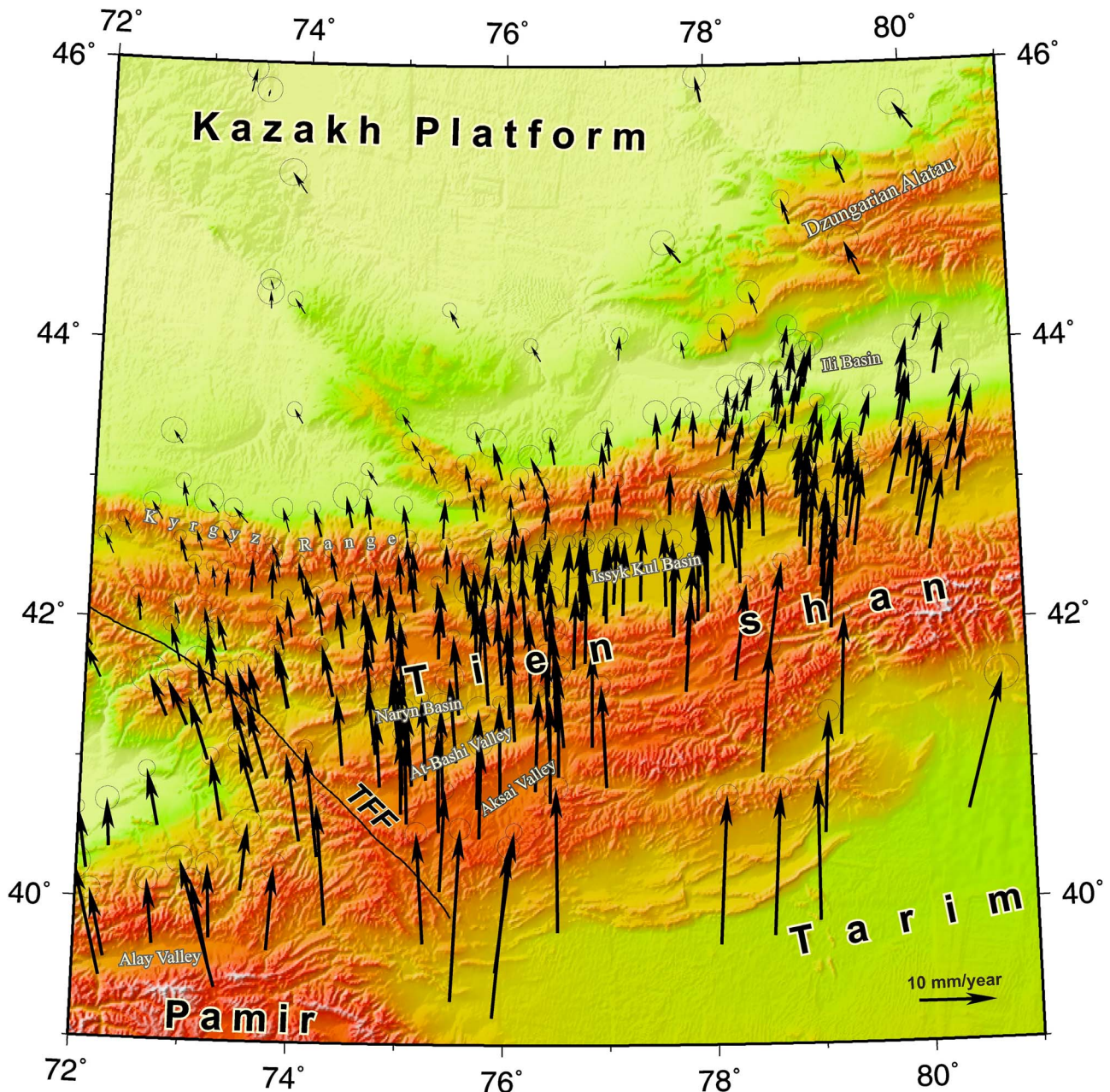
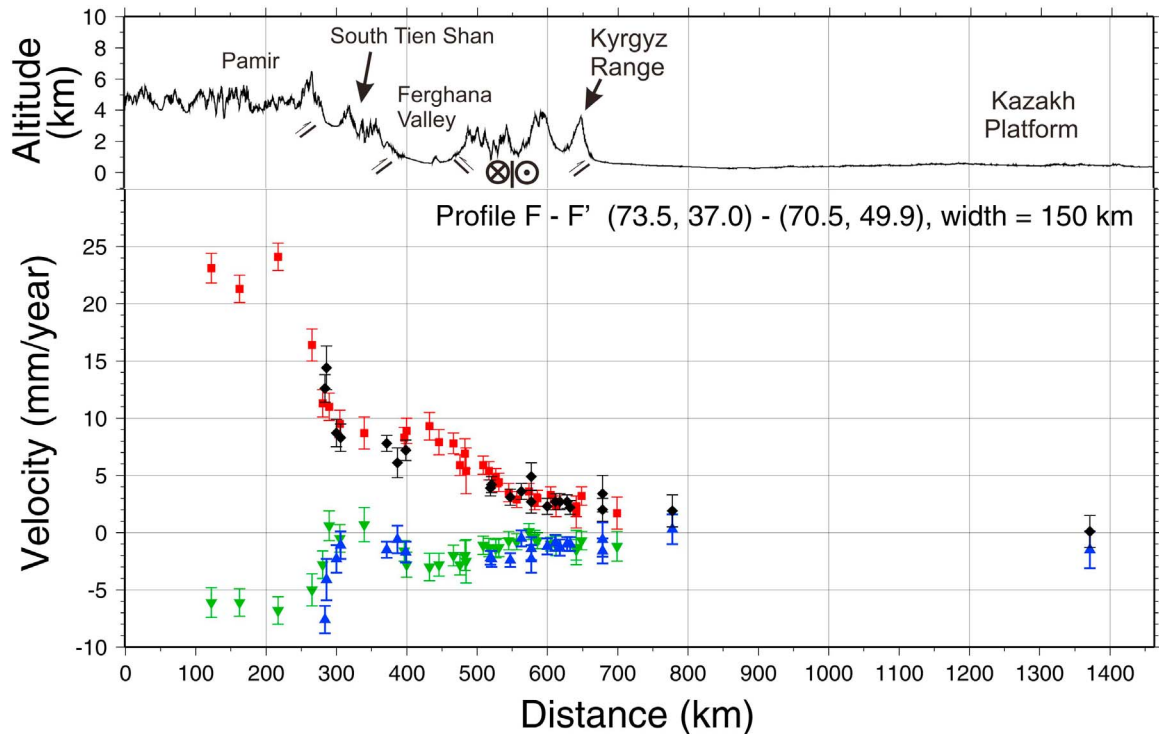


**Figure 6.** Map of Tien Shan with GPS velocities relative to Eurasia (box 1 in Figure 2). Error ellipses show 95% confidence ellipses.

along profile B-B' move with a left-lateral component of only  $\sim 2$  mm/yr (Figures 4 and 6). The left-lateral component on profile D-D' seems to be absorbed by shear in two zones, one (between 400 and 600 km) within the Tien Shan, and the other (near 800 km) at the edge of the Tien Shan and Ili Basin (Figures 2, 3, and 4d). On profile C-C', the left-lateral component seems to be absorbed by more localized shear than data on profile D-D' can resolve and again in two zones, one near the southern edge of the Issyk-Kul Basin, and the other at the edge of the Tien Shan and Ili Basin (Figures 3 and 4c). Localized shear zones are less clearly defined on profiles A-A' and B-B', in part because the

component of left-lateral shear along the Tien Shan is smaller there.

[22] The west to east increase in the left-lateral strike-slip component along the Tien Shan requires greater eastward components of velocity at sites in the eastern part of the Tien Shan than in the western part (Figures 3, 4, and 6). In the west, velocities are nearly parallel to profile A-A', but for profile D-D' in the east, they show clear eastward components. Thus, there might be a small ENE–WSW component of extension along and within the Tien Shan, despite the dominance of thrust faulting shown by fault plane solutions of nearly all earthquakes in the region [e.g., *Ghose et al.*,



Components of velocity parallel to the profile ( $\sim$ Northward):  $\blacklozenge$  (to left),  $\color{red}\blacksquare$  (to right from profile)  
 Components of velocity perpendicular to the profile ( $\sim$ Eastward):  $\color{blue}\blacktriangle$  (to left),  $\color{green}\blacktriangledown$  (to right from profile)

**Figure 7.** Profile of components of velocity across the Pamir, parts of Ferghana Valley and Tien Shan, and regions farther north relative to Eurasia (profile F-F' in Figure 2). Components perpendicular to the Alay Valley and Trans-Alay Range (and parallel to the profile) are shown with red squares and black diamonds, and components parallel to them (and perpendicular to profiles) are shown with blue and green triangles. Positive values show convergent (approximately northward) components, or movement to the right (approximately eastward). Error bars give  $1\sigma$  uncertainties. Black squares and blue upward pointing triangles show rates of points that lie within 75 km to the west, and red squares and green downward pointing triangles show points within 75 km to the east of profile F-F' in Figure 2. Thrust fault symbols are shown where active thrust faults have been mapped by *Arrowsmith and Strecker* [1999], inferred from seismicity [e.g., *Burtman and Molnar*, 1993], or from sharp breaks in the topography, and the position of the Talas-Ferghana strike-slip fault is inferred from its obvious expression in the topography.

1998; *Maggi et al.*, 2000; *Nelson et al.*, 1987; *Tapponnier and Molnar*, 1979] and by the absence of evidence of normal faulting. We presume that any extensional component of strain is accommodated by strike-slip faulting or shear on planes oriented obliquely to the belt.

### 3.4. The Pamir and Shortening Across the Alay Valley

[23] The network of GPS sites that we analyzed includes several sites in the northern part of the Pamir (Figures 2 and 3). Maximum north-northwestward components of velocity relative to Eurasia exceed those from the Tarim Basin (Figures 2 and 4). This difference in velocity would be consistent with a small component of right-lateral shear across the eastern part of the Pamir, where right-lateral faults have been mapped [e.g., *Cowgill*, 2010; *Peive et al.*, 1964; *Ruzhentsev*, 1963]. Such right-lateral shear might be present, but when south-southeastward components of ve-

locity are plotted on an east-northeast profile from the Pamir to the Tarim Basin (blue and green points on profile E-E'; Figure 5), no obvious step in rates is seen. Rather this component of velocity increases smoothly from east to west. Because the strike-slip component, which clearly exists in the southern Pamir, dies out to the north, it is possible that the GPS sites within the Pamir lie too far to the north to measure a strike-slip component.

[24] By contrast, east-northeastward components of velocity increase eastward, with a difference of 5–8 mm/yr between those within the Pamir and within the Tarim Basin (near 300 km on profile E-E'; Figure 5). Hence, the interior of the Pamir diverges from the Tarim Basin, despite the presence of folds and thrust faults along their boundary [e.g., *Jin et al.*, 2003]. This divergence attests to both east-west extension within the Pamir, a result consistent with fault plane solutions of earthquakes [e.g., *Burtman and Molnar*, 1993;

*Strecker et al.*, 1995], with the presence of grabens along the eastern part of the Pamir [e.g., *Cowgill*, 2010; *Tapponnier and Molnar*, 1979], and with velocities of a few continuous GPS sites in the Pamir and surroundings [*Mohadjer et al.*, 2010]. The folding of Mesozoic and Cenozoic sedimentary rock along the western edge of the Tarim Basin implies convergence perpendicular to the eastern margin of the Pamir [e.g., *Jin et al.*, 2003], but at present this convergence must be slow compared with the rate of divergence across a wider belt (Figure 5). We are unaware of evidence that constrains either when the divergence began or when convergence on the eastern margin occurred most rapidly.

[25] Because of the paucity of GPS sites within the Pamir, its deformation field cannot be quantified in full. Nevertheless, as shown by profile F-F' (Figures 2 and 7), rates relative to Eurasia decrease by at least 10 and possibly by 15 mm/yr over a short distance that spans the Trans-Alay Range (near 250 km; Figure 7), which marks the northern margin of the Pamir, and the Alay Valley just to its north. Although the rotation of the Ferghana Valley relative to Eurasia (discussed below) can account for ~5 mm/yr of nearly ~25 mm/yr of north-northwestward convergence of the central Pamir with Eurasia, it appears that thrust faulting at the northern margin of the Pamir absorbs at least 10 and maybe 15 mm/yr of that ~25 mm/yr of convergence between the Pamir and Eurasia. Such a rate is similar to the  $13 \pm 4$  mm/yr that *Reigber et al.* [2001] had inferred, and consistent with triangulation measurements made farther west [e.g., *Guseva*, 1986; *Konopaltsev*, 1971a, 1971b].

[26] Most, if not all, of this convergence between the Pamir and Eurasia may be absorbed at the system of thrust faults in the Alay Valley. The high level of seismicity in this region attests to localized deformation (Figure 1), and evidence of thrust faulting in this region abounds [e.g., *Coutand et al.*, 2002; *Nikonov*, 1974, 1975, 1977; *Nikonov et al.*, 1983; *Strecker et al.*, 2003]. *Arrowsmith and Strecker* [1999] measured a lower bound of 6 mm/yr for Holocene convergence at one location near 39.5°N, 72.6°E. The GPS measurements reported here suggest that localized convergence may be much more rapid than just 6 mm/yr, and perhaps occurs by slip on more than one thrust, or reverse, fault in this region. Obviously, with so few measurement points we cannot eliminate north-south crustal shortening within the Pamir as well, but both fault plane solutions of earthquakes and evidence of active faulting imply a preponderance of normal faulting and east-west extension within the high axial portion of the Pamir [e.g., *Burtman and Molnar*, 1993; *Strecker et al.*, 1995]. Thus, we doubt that reverse faulting and contraction at more than a couple of mm/yr occurs in this region.

[27] This zone of thrust or reverse faulting along the Trans-Alay Range seems to mark a zone of intracontinental subduction [e.g., *Burtman and Molnar*, 1993; *Chatelain et al.*, 1980; *Hamburger et al.*, 1992], where the eastern continuation of the Tajik Depression has been subducted southward beneath the Pamir. The suggestion of localized deformation at the foot of the Trans-Alay Range, therefore, accords with this region being the surface manifestation of such subduction.

### 3.5. Rotation of the Ferghana Valley and Slip on the Talas-Ferghana Fault

[28] West of the segment of the Tien Shan that separates the effectively rigid Tarim Basin from the Kazakh Platform to the north, the high terrain of the Tien Shan west of the Talas-Ferghana fault splits into two belts that surround the Ferghana Valley, which also seems to behave as a block that deforms at most only slowly (Figures 2 and 8). With thick, poorly consolidated sedimentary rock, the Ferghana Valley offers poor sites for GPS points, and most sites have been installed in sedimentary rock exposed in folds on the margins of the valley. Rates of movement relative to Eurasia increase from low rates at sites in the southwestern part of the basin to higher rates near its northeast margin, consistent with rotation of the basin, with respect to Eurasia, about an axis near its southwest end [e.g., *Reigber et al.*, 2001; *Thomas et al.*, 1993]. Sites on the southeast side, however, move faster toward Eurasia than those on the northwest side, presumably because they lie within the deforming margins of the Ferghana Valley. On the northwest margin, crustal shortening occurs with a NW-SE orientation, and on its southern margin, north-south shortening occurs. Field observations, geophysical profiling, and fault plane solutions of earthquakes suggest that the east-west trending South Tien Shan, which is cored largely by Paleozoic metamorphic rock, has been thrust atop the southern edge of the Ferghana Valley [e.g., *Burtman and Molnar*, 1993; *Laverov and Makarov*, 2005]. Thus, the counterclockwise rotation of the Ferghana Valley converts roughly north-south movement of the South Tien Shan with respect to Eurasia, into NW-SE shortening across the Chatkal and adjacent ranges that lie northwest of the valley. Using sites on the margins of the Ferghana Valley and allowing uniform strain among them, we estimate an angular velocity of the valley with respect to Eurasia given by counterclockwise rotation at  $-0.73^\circ (\pm 0.08^\circ) \text{ Myr}^{-1}$  about an axis of rotation that is located just southwest of the valley at 39.9°N ( $\pm 0.4$ ), 67.5°E ( $\pm 0.7$ ) (Figure 8). To determine that angular velocity, we used those points shown in Figure 8 with blue arrows superimposed on them; the blue arrows show calculated velocities for those points.

[29] The eastern end of the Ferghana Valley is bounded by high terrain through which a clear right-lateral strike-slip fault passes, the Talas-Ferghana fault [e.g., *Burtman*, 1963, 1964, 1975]. From several upper bounds of ~10 mm/yr for the Holocene slip rate on the fault, *Burtman et al.* [1996] suggested that the fault currently slips at that rate. By contrast, *Trifonov et al.* [1992] inferred that Late Quaternary and Holocene right-lateral slip along the fault was not uniform along the fault, and that the highest rate of about 15 mm/yr occurs in its central part just opposite the Ferghana Valley. GPS data, however, including both analyses of a subset of the data that we present here [e.g., *Meade and Hager*, 2001; *Zubovich et al.*, 2007] and of other, independent data [*Mohadjer et al.*, 2010], showed that the rate must be much lower,  $< \sim 2$  mm/yr. The modest differences in velocities of sites on the two sides of the fault (Figures 8 and 9) demonstrate that the slip rate indeed is small, no more than ~1–2 mm/yr. Profiles of GPS velocities (Figure 9), in

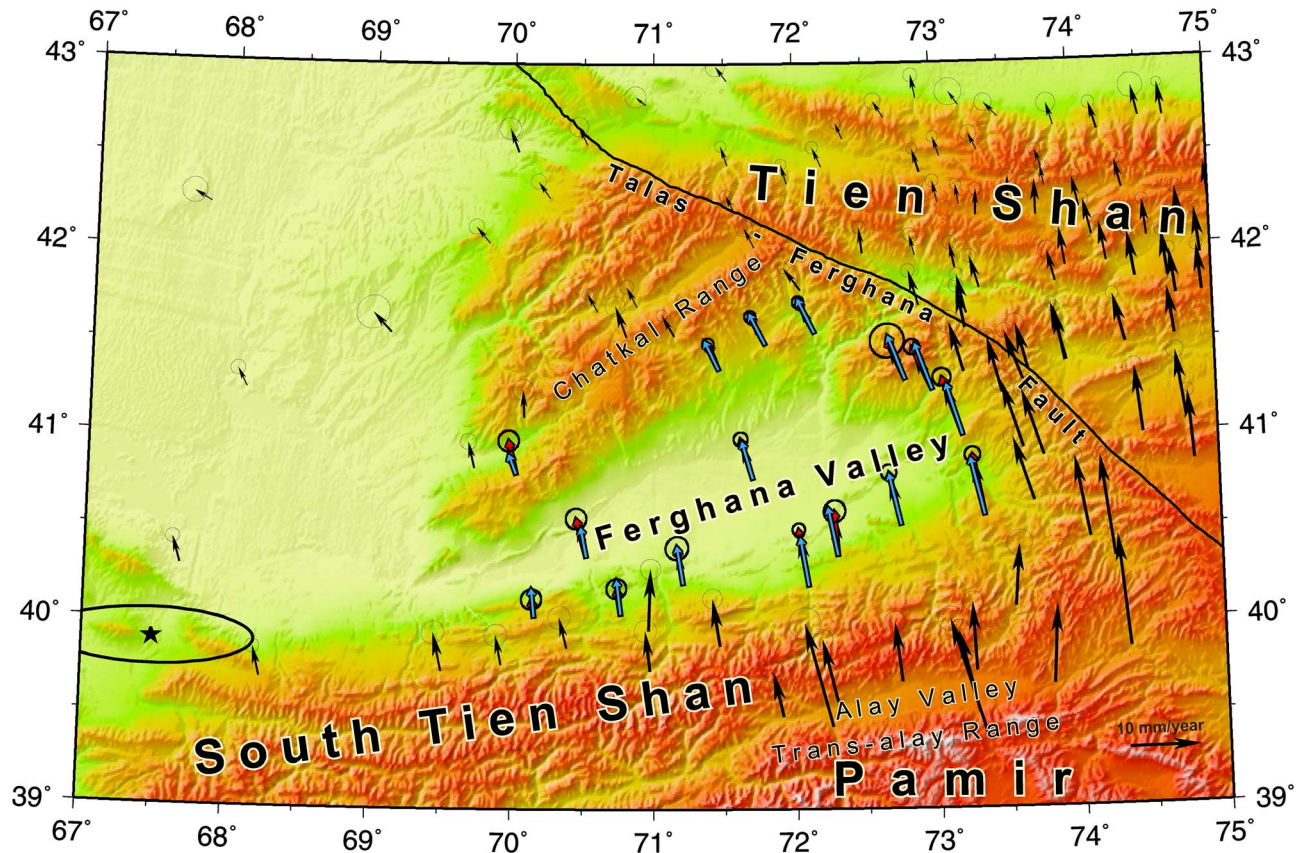


**Figure 8.** Map of Ferghana Valley and surrounding region with GPS velocities (black and red arrows) relative to Eurasia (region 2 in Figure 2). Red arrows show points that are assumed to be part of the Ferghana Valley, and blue arrows show velocities calculated assuming that the region including those points (1) contracts at rates of  $15 \times 10^{-9} \text{ yr}^{-1}$  oriented  $\text{N}157^\circ\text{E}$ , and at  $1.5 \times 10^{-9} \text{ yr}^{-1}$  at  $\text{N}67^\circ\text{E}$ , and (2) rotates about an axis at  $67.5^\circ\text{E} \pm 0.7^\circ\text{E}$ ,  $39.9^\circ\text{N} \pm 0.4^\circ\text{N}$  at a rate of  $-0.73^\circ \pm 0.08^\circ \text{ Myr}^{-1}$  with respect to Eurasia. Error ellipses show 95% confidence regions.

fact, give little indication of any slip at all. Moreover, the obliquity of the fault to the direction of movement of the Ferghana Valley, relative to Eurasia, attest to a small component of convergence perpendicular to the fault, which presumably manifests itself, at least in part, in the presence of high terrain southwest of the fault.

#### 4. Conclusions

[30] The GPS data presented here demonstrate that the western part of the Tarim Basin converges with Eurasia at  $20 \pm 2 \text{ mm/yr}$  (Figures 2 and 4, profiles A-A' and B-B'), where convergence between India and Eurasia is only  $\sim 33 \text{ mm/yr}$  [Argus et al., 2010]. At a convergence rate of  $20 \text{ mm/yr}$  the entire Tien Shan would have been built in less than 10 Ma. Thus, these data suggest that following slow initial growth, the Tien Shan did not develop into a major mountain belt until late in the history of convergence between India and Eurasia [Abdrakhmatov et al., 1996; Reigber et al., 2001].

[31] Most of the convergence between the Tarim Basin and the Kazakh Platform is absorbed within the Tien Shan, presumably by slip on thrust or reverse faults; localized

zones of shortening at rates of  $\sim 2 \text{ mm/yr}$  to as many as  $6 \text{ mm/yr}$  lie within the Tien Shan. In addition, shortening at  $\sim 1\text{--}3 \text{ mm/yr}$  occurs north of the belt, within the Dzungarian Alatau and its westward continuation, and possibly also in the southern part of the Kazakh Platform. Moreover, the movement of the Tarim Basin toward the Kazakh Platform includes a left-lateral strike-slip component parallel to the Tien Shan of  $\sim 4 \text{ mm/yr}$  in the eastern part of our network, decreasing to only  $\sim 2 \text{ mm/yr}$  at the western end of the belt, which we associate with clockwise rotation of the Tarim Basin with respect to Eurasia.

[32] GPS data surrounding the Ferghana Valley corroborate the inference that this basin has rotated around an axis southwest of the valley [Reigber et al., 2001; Thomas et al., 1993], and refine the angular velocity of that motion (Figure 8). Shortening across the Chatkal and parallel mountain ranges that lie along the northwestern margin of the valley occurs at  $\sim 5 \text{ mm/yr}$ . Slip on the Talas-Ferghana fault, at the eastern end of the Ferghana Valley, occurs at  $< 2 \text{ mm/yr}$  (Figure 9) [Meade and Hager, 2001; Mohadjer et al., 2010; Zubovich et al., 2007].

[33] Convergence between the Tarim Basin and the Kazakh Platform is absorbed over a region more than 200 km wide,

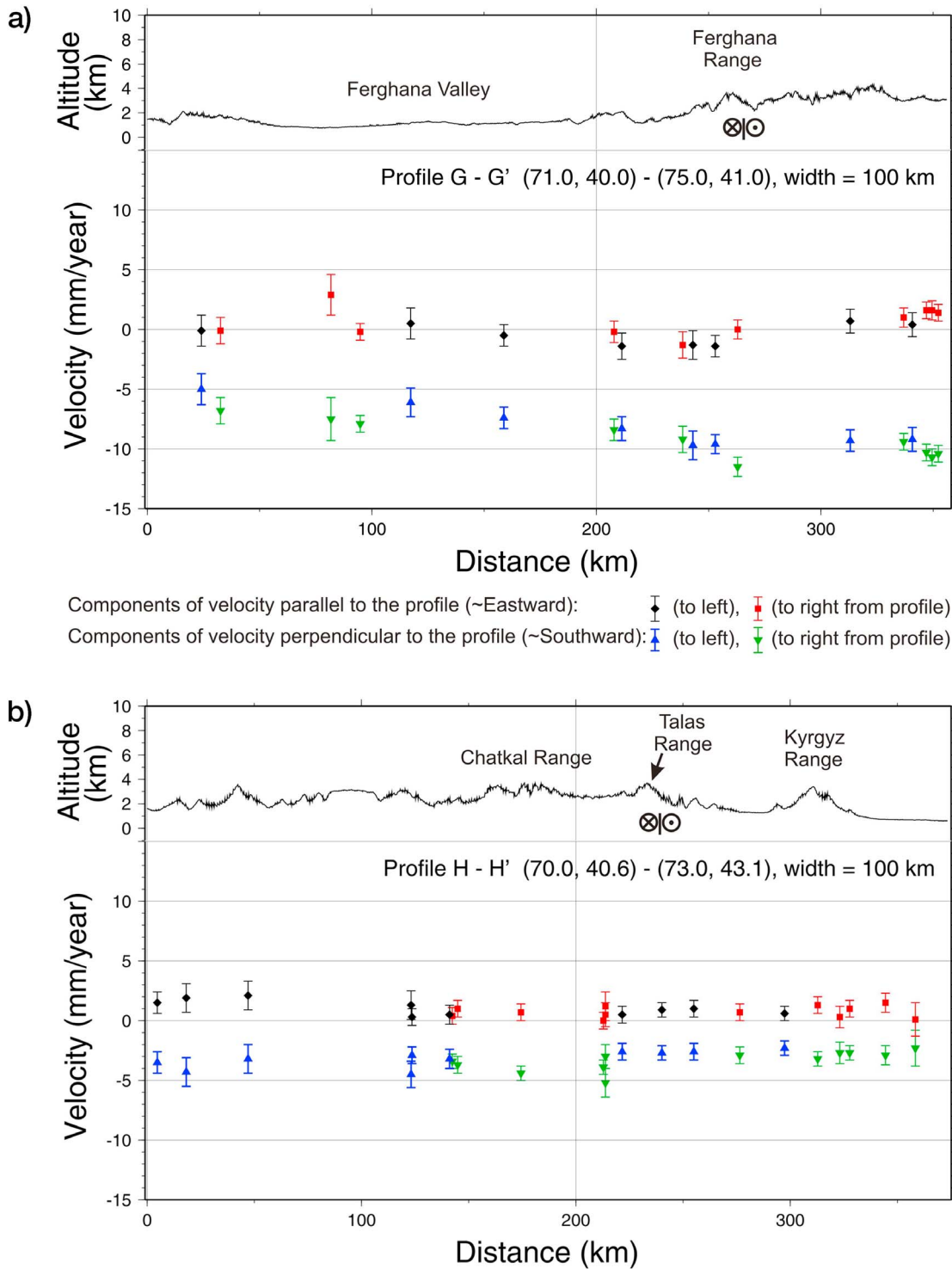


**Figure 9.** Profiles of components of velocity across the Ferghana Valley, Talas-Ferghana fault, and western Tien Shan relative to Eurasia (profiles G-G' and H-H' in Figure 2). Positive values for black diamonds and red squares indicate approximately eastward components, and those for blue and green triangles show movement to the right of the profiles, approximately southward. Error bars give  $1\sigma$  uncertainties. Black diamonds and blue upward pointing triangles show rates for points within 75 km to the north of profiles G-G' and H-H' in Figure 2, and red squares and green downward pointing triangles show points within 75 km to the south of those profiles. Symbols showing strike-slip faulting indicate the position of the Talas-Ferghana fault, as inferred from the detailed topography.

and although it is not uniformly distributed, no single predominant fault absorbs the majority of this convergence. By contrast, the Pamir seems to move northward toward Eurasia with a large fraction absorbed near the Alay Valley, which lies just north of the Trans-Alay Range and bounds the northern edge of the Pamir. The shortening rate in this zone is at least 10 and perhaps 15 mm/yr, similar to what *Reigber et al.* [2001] had inferred from fewer measurements. Moreover, the northern part of the Pamir diverges westward from the Tarim Basin at 5–8 mm/yr, a result consistent with the presence of grabens in the eastern Pamir, with fault plane solutions of earthquakes that demonstrate normal faulting and east–west extension, and with sparse continuous GPS measurements [*Mohadjer et al.*, 2010].

## Appendix A: Processing of GPS Observations

[34] We analyzed the GPS data using the GAMIT/GLOBK software [*Herring*, 2004; *King and Bock*, 2004] with a three-step approach [*Dong et al.*, 1998, *Herring et al.*, 2002]. In the first step, for each day we used GPS phase observations to estimate station coordinates and the zenith delay of the atmosphere at each station that recorded GPS signal that day, and parameters describing the orbits of the satellites and the orientation of the Earth. To tie the regional measurements to an external global reference frame in the next steps, we included 8–12 continuously operating IGS stations in the processing of data for each day [*Dow et al.*, 2009]. In the second step, we combined the regional daily solutions from the first step with global GPS analysis performed at Scripps Institution of Oceanography and saved them into a single file, for each campaign, as loosely constrained solutions of site positions. The Scripps global analysis contains over 300 stations and provides accurate orbits and positions of these stations.

[35] In the third step, the combined loosely constrained solutions for each campaign were passed through a Kalman filter, GLOBK [*Herring*, 2004], to estimate a consistent set of coordinates and velocities. Before we estimated velocities, however, we examined time series of positions obtained in the two earlier steps to identify outliers and offsets or “jumps.” We removed outlier position estimates from the solution and covariance matrices used in the GLOBK Kalman filter analysis, and we accounted for offsets by allowing independent position estimates before and after the time of

the offset. We used random walk variances of 1–4 mm<sup>2</sup>/yr<sup>2</sup> in the forward run of the GLOBK Kalman filter estimate site velocities and “realistic” uncertainties. Except where indicated otherwise, we quote uncertainties as 1-sigma estimates (Table 1), but in Figures 3, 6, and 8 we show 95% confidence ellipses.

[36] We defined the reference frame for velocity estimates in the third step, when we applied generalized constraints [*Dong et al.*, 1998] and estimated the six parameters (three components of the rate of change of translation, three for rotation) that tie that reference frame to a global frame. In particular, we determined those six parameters by minimizing the horizontal velocities of 55 stable global IGS stations with respect to the ITRF2005 NNR frame and the rotated ITRF2005 EURA frame using the ITRF2005 angular velocity [*Altamimi et al.*, 2007; *Herring et al.*, 2009]. The weighted RMS fit of the horizontal velocities to the ITRF 2005 EURA frame using 52 global sites as reference sites was 0.4 mm/yr. In Table 1, we present these velocities and associated 1-sigma standard deviations.

[37] **Acknowledgments.** Many people have contributed to the installation, maintenance, and measurement of the network, from its inception to the latest measurements, but one person, Yuri A. Trapeznikov, played a particularly important role before he died in 1999. A pioneer in GPS geodetic measurements in the former Soviet Union, he obtained permission to install GPS points, created the facilities to record and analyze data, orchestrated ambitious field campaigns, helped design the “Russian” mark, and made sure that the GPS network in the Kyrgyz and Kazakh Tien Shan became one of the best in the world. We also express special thanks to J. Klotz for the design of the “German” mark and many CATS site installations. Although many more people helped us than we can mention here, we thank K. Ye. Abdrakhmatov, S. A. Aldazhanov, D. Angermann, R. Arslanov, B. N. Bakka, J. Y. Chen, R. Galas, T. V. Guseva, M. C. Ishanov, K. B. Kalabaev, G. W. Michel, M. T. Prilepin, I. S. Sadybakasov, V. Ye. Tsurkov, and P. V. Yeremeyev for help and support of various kinds. We also thank A. K. Rybin and V. A. Zeigarnik, current and former directors of the Research Station, and H. Ehtler and B. Moldobekov, codirectors of CAIAG, for encouraging and helping us to present these GPS data, and D. W. Burbank and P. C. England for constructive reviews of the paper. This research was supported by the Russian Foundation for Basic Research of the Russian Academy of Sciences, Russian Federation; by the National Science Foundation under grants EAR-8915334, EAR-9117889, EAR-9614302, EAR-9708618, and EAR-0636092, by NASA through grants NAG5-1941 and NAG5-1947; by the Deutsches GeoForschungsZentrum in Potsdam; by the National Bureau of Surveying and Mapping (NBSM) in Beijing and Urumqi; and by the staff of the UNAVCO Facility for expert field engineering support and data archiving.

## References

- Abdrakhmatov, K. E., R. Weldon, S. Thompson, D. Burbank, C. Rubin, M. Miller, and P. Molnar (2001), Origin, direction, and rate of modern compression in the central Tien Shan, Kyrgyzstan, *Geol. Geofiz.*, *42*, 1585–1609.
- Abdrakhmatov, K. E., S. Thompson, and R. Weldon (2007), *Active Tectonics of the Tien Shan* (in Russian), 71 pp., Ilim, Bishkek.
- Abdrakhmatov, K. Y., et al. (1996), Relatively recent construction of the Tien Shan inferred from GPS measurements of present-day crustal deformation rates, *Nature*, *384*, 450–453, doi:10.1038/384450a0.
- Altamimi, Z., X. Collilieux, J. LeGrand, B. Garayt, and C. Boucher (2007), ITRF2005: A new release of the International Terrestrial Reference Frame based on time series of station positions and Earth Orientation Parameters, *J. Geophys. Res.*, *112*, B09401, doi:10.1029/2007JB004949.
- Argus, D. F., R. G. Gordon, M. B. Heflin, C. Ma, R. J. Eanes, P. Willis, W. R. Peltier, and S. E. Owen (2010), The angular velocities of the plates and the velocity of Earth’s centre from space geodesy, *Geophys. J. Int.*, *180*, 913–960, doi:10.1111/j.1365-246X.2009.04463.x.
- Arrowsmith, J. R., and M. R. Strecker (1999), Seismotectonic range-front segmentation and mountain-belt growth in the Pamir–Alai region, Kyrgyzstan (India–Eurasia collision zone), *Geol. Soc. Am. Bull.*, *111*, 1665–1683, doi:10.1130/0016-7606(1999)111<1665:SRFSAM>2.3.CO;2.
- Avouac, J. P., P. Tapponnier, M. Bai, H. You, and G. Wang (1993), Active thrusting and folding along the northern Tien Shan and Late Cenozoic rotation of the Tarim relative to Dzungaria and Kazakhstan, *J. Geophys. Res.*, *98*, 6755–6804, doi:10.1029/92JB01963.
- Bazhenov, M. L. (1993), Cretaceous paleomagnetism of the Fergana Basin and adjacent ranges, central Asia: Tectonic implications, *Tectonophysics*, *221*, 251–267, doi:10.1016/0040-1951(93)90335-H.
- Bogomolov, L., V. Bragin, A. Fridman, V. Makarov, G. Sobolev, E. Polyachenko, G. Schelochkov, V. Zeigarnik, and A. Zubovich (2007), Comparative analysis of GPS, seismic and electromagnetic data on the central Tien Shan territory, *Tectonophysics*, *431*, 143–151, doi:10.1016/j.tecto.2006.05.043.
- Bragin, V. D., V. Y. Batalev, A. V. Zubovich, A. N. Lobanenko, A. K. Rybin, Y. A. Trapeznikov, and G. G. Schelochkov (2001), Signature of neotectonic movements in the geoelectric structure of the

- crust and seismicity distribution in the central Tien Shan, *Russ. Geol. Geophys.*, 42, 1527–1537.
- Bullen, M. E., D. W. Burbank, J. I. Garver, and K. Y. Abdрахmatov (2001), Late Cenozoic tectonic evolution of the northwestern Tien Shan: New age estimates for the initiation of mountain building, *Geol. Soc. Am. Bull.*, 113, 1544–1559, doi:10.1130/0016-7606(2001)113<1544:LCTEOT>2.0.CO;2.
- Bullen, M. E., D. W. Burbank, and J. I. Garver (2003), Building the northern Tien Shan: Integrated thermal, structural, and topographic constraints, *J. Geol.*, 111, 149–165, doi:10.1086/345840.
- Burtman, V. S. (1963), The Talaso-Fergana and San Andreas strike-slip faults, in *Faults and Horizontal Movements of the Earth's Crust* (in Russian), edited by A. V. Peive, *Tr. Geol. Inst. Akad. Nauk USSR*, 80, 128–151.
- Burtman, V. S. (1964), *The Talaso-Fergana Strike-Slip Fault* (in Russian), *Tr. Geol. Inst. Akad. Nauk USSR*, 104, 143 pp.
- Burtman, V. S. (1975), Structural geology of the Variscan Tien Shan, USSR, *Am. J. Sci.*, 272A, 157–186.
- Burtman, V. S., and P. Molnar (1993), *Geological and Geophysical Evidence for Deep Subduction of Continental Crust Beneath the Pamir*, *Spec. Pap. Geol. Soc. Am.*, 281, 76 pp.
- Burtman, V. S., S. F. Skobelev, and P. Molnar (1996), Late Cenozoic slip on the Talas-Fergana fault, the Tien Shan, central Asia, *Geol. Soc. Am. Bull.*, 108, 1004–1021, doi:10.1130/0016-7606(1996)108<1004:LCSTOT>2.3.CO;2.
- Calais, E., L. Dong, M. Wang, Z. Shen, and M. Vergnolle (2006), Continental deformation in Asia from a combined GPS solution, *Geophys. Res. Lett.*, 33, L24319, doi:10.1029/2006GL028433.
- Charreau, J., Y. Chen, S. Gilder, S. Dominguez, J.-P. Avouac, S. Sen, D. Sun, Y. Li, and W.-M. Wang (2005), Magnetostratigraphy and rock magnetism of the Neogene Kuitun He section (northwest China): Implications for Late Cenozoic uplift of the Tianshan mountains, *Earth Planet. Sci. Lett.*, 230, 177–192, doi:10.1016/j.epsl.2004.11.002.
- Charreau, J., S. Gilder, Y. Chen, S. Dominguez, J.-P. Avouac, S. Sen, M. Jolivet, Y. Li, and W. Wang (2006), Magnetostratigraphy of the Yaha section, Tarim Basin (China): 11 Ma acceleration in erosion and uplift of the Tianshan mountains, *Geology*, 34, 181–184, doi:10.1130/G22106.1.
- Charreau, J., J.-P. Avouac, Y. Chen, S. Dominguez, and S. Gilder (2008), Miocene to present kinematics of fault-bend folding across the Huerquosi anticline, northern Tianshan (China), derived from structural, seismic, and magnetostratigraphic data, *Geology*, 36, 871–874, doi:10.1130/G25073A.1.
- Charreau, J., et al. (2009), Neogene uplift of the Tien Shan Mountains observed in the magnetic record of the Jingou River section (northwest China), *Tectonics*, 28, TC2008, doi:10.1029/2007TC002137.
- Chatelain, J.-L., S. W. Roecker, D. Hatzfeld, and P. Molnar (1980), Microearthquake seismicity and fault plane solutions in the Hindu Kush region and their tectonic implications, *J. Geophys. Res.*, 85, 1365–1387, doi:10.1029/JB085iB03p01365.
- Chedia, O. K. (1986), *Morphostructures and Neotectonics of the Tien Shan* (in Russian), 314 pp., ILIM, Frunze, Kyrgyzstan.
- Cobbold, P. R., E. Sadybakasov, and J. C. Thomas (1996), Cenozoic transpression and basin development, Kyrgyz Tianshan, central Asia, in *Geodynamic Evolution of Sedimentary Basins*, edited by F. Roure et al., pp. 181–202, Ed. Technip, Paris.
- Coutand, I., M. R. Strecker, J. R. Arrowsmith, G. Hilley, R. C. Thiede, A. Korjenkov, and M. Omuraliev (2002), Late Cenozoic tectonic development of the intramontane Alai Valley, (Pamir-Tien Shan region, central Asia): An example of intracontinental deformation due to the Indo-Eurasia collision, *Tectonics*, 21(6), 1053, doi:10.1029/2002TC001358.
- Cowgill, E. (2010), Cenozoic right-slip faulting along the eastern margin of the Pamir salient, northwestern China, *Geol. Soc. Am. Bull.*, 122, 145–161, doi:10.1130/B26520.1.
- Dong, D., T. A. Herring, and R. W. King (1998), Estimating regional deformation from a combination of space and terrestrial geodetic data, *J. Geod.*, 72, 200–214, doi:10.1007/s001900050161.
- Dow, J. M., R. E. Neilan, and C. Rizos (2009), The International GNSS Service in a changing landscape of global navigation satellite systems, *J. Geod.*, 83, 191–198, doi:10.1007/s00190-008-0300-3.
- Engdahl, E. R., R. van der Hilst, and R. Buland (1998), Global teleseismic earthquake relocation with improved travel times and procedures for depth determination, *Bull. Seismol. Soc. Am.*, 88, 722–743.
- England, P., and P. Molnar (2005), Late Quaternary to decadal velocity fields in Asia, *J. Geophys. Res.*, 110, B12401, doi:10.1029/2004JB003541.
- Garzanti, E., and T. Van Haver (1988), The Indus clastics: Forearc basin sedimentation in the Ladakh Himalaya (India), *Sediment. Geol.*, 59, 237–249, doi:10.1016/0037-0738(88)90078-4.
- Ghose, S., M. W. Hamburger, and C. J. Ammon (1998), Source parameters of moderate-sized earthquakes in the Tien Shan, central Asia from regional moment tensor inversion, *Geophys. Res. Lett.*, 25, 3181–3184, doi:10.1029/98GL02362.
- Gu, G., T. Lin, Z. Shi, Q. Li, H. Wu, S. Li, Y. Yang, H. Chen, and S. Wang (Eds.) (1989), *Catalogue of Chinese Earthquakes (1831 B. C.–1969 A. D.)*, 872 pp., Science, Beijing.
- Guseva, T. G. (1986), *Contemporary Movements of the Earth's Crust in the Transition Zone From the Pamir to the Tien Shan* (in Russian), 171 pp., Inst. Phys. Earth, Akad. Sci., Moscow.
- Hamburger, M. W., D. R. Sarewitz, T. L. Pavlis, and G. A. Popandopulo (1992), Structural and seismic evidence for intracontinental subduction in the Peter the First Range, central Asia, *Geol. Soc. Am. Bull.*, 104, 397–408, doi:10.1130/0016-7606(1992)104<0397:SASEFI>2.3.CO;2.
- Heermance, R. V., J. Chen, D. W. Burbank, and J. Miao (2008), Temporal constraints and pulsed Late Cenozoic deformation during the structural disruption of the active Kashi foreland, northwest China, *Tectonics*, 27, TC6012, doi:10.1029/2007TC002226.
- Hendrix, M. S., T. A. Dumitru, and S. A. Graham (1994), Late Oligocene–early Miocene unroofing in the Chinese Tien Shan: An early effect of the India-Eurasia collision, *Geology*, 22, 487–490, doi:10.1130/0091-7613(1994)022<0487:LOE-MUI>2.3.CO;2.
- Herring, T. A. (2004), *GLOBK: Global Kalman Filter VLB1 and GPS Analysis Program Version 4.1*, Mass. Inst. of Technol., Cambridge.
- Herring, T. A., B. H. Hager, B. Meade, and A. V. Zubovich (2002), Contemporary horizontal and vertical deformation in the Tien Shan, paper presented at International Seminar on the Use of Space Techniques for Asia-Pacific Regional Crustal Movements Studies, GEOS, Moscow.
- Herring, T. A., R. W. King, and S. C. McClusky (2009), Introduction to GAMIT/GLOBK, *Release 10.35*, Mass. Inst. of Technol., Cambridge.
- Huang, B., J. D. A. Piper, S. Peng, T. Liu, Z. Li, Q. Wang, and R. Zhu (2006), Magnetostratigraphic study of the Kuche Depression, Tarim Basin, and Cenozoic uplift of the Tien Shan Range, western China, *Earth Planet. Sci. Lett.*, 251, 346–364, doi:10.1016/j.epsl.2006.09.020.
- Huang, B., J. D. A. Piper, Q. Qiao, H. Wang, and C. Zhang (2010), Magnetostratigraphic and rock magnetic study of the Neogene upper Yaha section, Kuche Depression (Tarim Basin): Implications to formation of the Xiyu conglomerate formation, NW China, *J. Geophys. Res.*, 115, B01101, doi:10.1029/2008JB006175.
- Jade, S., B. C. Bhatt, R. Bendick, V. K. Gaur, P. Molnar, M. B. Anand, and D. Kumar (2004), GPS measurements from the Ladakh Himalaya, India: Preliminary tests of plate-like or continuous deformation in Tibet, *Geol. Soc. Am. Bull.*, 116, 1385–1391, doi:10.1130/B25357.1.
- Ji, J., P. Luo, P. White, H. Jiang, L. Gao, and Z. Ding (2008), Episodic uplift of the Tianshan Mountains since the late Oligocene constrained by magnetotratigraphy of the Jingou River section, in the southern margin of the Junggar Basin, China, *J. Geophys. Res.*, 113, B05102, doi:10.1029/2007JB005064.
- Jin, X., J. Wang, B. Chen, and L. Ren (2003), Cenozoic deposits in the piedmont of the west Kunlun and their paleogeographic and tectonic implications, *J. Asian Earth Sci.*, 21, 755–765, doi:10.1016/S1367-9120(02)00073-1.
- King, R. W., and Y. Bock (2004), *Documentation of the MIT GPS Analysis Software: GAMIT*, Mass. Inst. of Technol., Cambridge.
- Kondorskaya, N. V., and N. V. Shebalin (Eds.) (1977), *New Catalog of Strong Earthquakes in the Territory of the USSR* (in Russian), 535 pp., Nauka, Moscow.
- Konopaltsev, I. M. (1971a), Measurement of movement of the Earth's crust in the Garm polygon (in Russian), *Izv. Akad. Nauk, Fiz. Zemlyi*, 6, 71–76.
- Konopaltsev, I. M. (1971b), Measurements of crustal movements in the Garm area, 1948–1970 (in Russian), *Geotektonika*, 5, 111–116.
- Kosarev, G. L., N. V. Petersen, L. P. Vinnik, and S. W. Roecker (1993), Receiver functions for the Tien Shan analog broadband network: Contrasts in the evolution of the structures across the Talaso-Fergana fault, *J. Geophys. Res.*, 98, 4437–4448, doi:10.1029/92JB02651.
- Kreydenkov, G. P., and V. A. Raspopin (1972), Paleogene of southern Kirgizia, in *Geology of the USSR*, vol. 25, *Kirgiz SSR: Geological Description—Book 1*, edited by K. D. Pomazkov et al., pp. 237–250, Nedra, Moscow.
- Kuzichkina, Y. M. (1972), Jurassic system, in *Geology of the USSR*, vol. 25, *Kirgiz SSR: Geological Description—Book 1*, edited by K. D. Pomazkov et al., pp. 208–224, Nedra, Moscow.
- Kuzikov, S. I., and S. A. Mukhamediev (2010), Structure of the present-day velocity field of the crust in the area of the central Asian GPS network, *Izv. Phys. Solid Earth*, 46(7), 584–601, doi:10.1134/S1069351310070037.
- Laverov, N. P., and V. I. Makarov (Eds.) (2005), *Recent Geodynamics of Intracontinental Areas of Collision Mountain Building (Central Asia)*, 400 pp., Sci. World, Moscow.
- Li, Z., S. Roecker, Z. Li, B. Wei, H. Wang, G. Schelochkov, and V. Bragin (2009), Tomographic image of the crust and upper mantle beneath the western Tien Shan from the MANAS broadband deployment: Possible evidence for lithospheric delamination, *Tectonophysics*, 477, 49–57, doi:10.1016/j.tecto.2009.05.007.
- Maggi, A., J. A. Jackson, K. Priestley, and C. Baker (2000), A re-assessment of focal depth distributions in southern Iran, the Tien Shan and northern India: Do earthquakes really occur in the continental mantle?, *Geophys. J. Int.*, 143, 629–661, doi:10.1046/j.1365-246X.2000.00254.x.
- Makarov, V. I. (1977), *New Tectonic Structures of the Central Tien Shan* (in Russian), vol. 307, 171 pp., Order of the Red Banner Geol. Inst., Akad. Sci., Moscow.
- Makarov, V. I. (1995), Neotectonics and geodynamics of mountain systems of central Asia, *Quat. Int.*, 25, 19–23, doi:10.1016/1040-6182(94)00031-Y.
- Makarov, V. I., et al. (2010), Underthrusting of Tarim beneath the Tien Shan and deep structure of their junction zone: Main results of seismic experiment along MANAS Profile Kashgar–Song–K6l (in Russian), *Geotektonika*, 44, 23–42. (*Geotectonics*, Engl. Transl., 44, 102–126.)
- Meade, B. J. (2007), Present-day kinematics at the India-Asia collision zone, *Geology*, 35, 81–84, doi:10.1130/G22924A.1.
- Meade, B. J., and B. H. Hager (2001), The current distribution of deformation in the western Tien Shan from block models constrained by geodetic data, *Geol. Geofiz.*, 42, 1622–1633.
- Mellors, R. J., G. L. Pavlis, M. W. Hamburger, H. J. Al-Shukri, and A. A. Lukk (1995), Evidence for a high-velocity slab associated with the Hindu Kush

- seismic zone, *J. Geophys. Res.*, **100**, 4067–4078, doi:10.1029/94JB02642.
- Mohadjer, S., et al. (2010), Partitioning of India-Eurasia convergence in the Pamir-Hindu Kush from GPS measurements, *Geophys. Res. Lett.*, **37**, L04305, doi:10.1029/2009GL041737.
- Molnar, P., and Q. Deng (1984), Faulting associated with large earthquakes and the average rate of deformation in central and eastern Asia, *J. Geophys. Res.*, **89**, 6203–6227, doi:10.1029/JB089iB07p06203.
- Molnar, P., and S. Ghose (2000), Seismic moments of major earthquakes and the rate of shortening across the Tien Shan, *Geophys. Res. Lett.*, **27**, 2377–2380, doi:10.1029/2000GL011637.
- Nelson, M. R., R. McCaffrey, and P. Molnar (1987), Source parameters for 11 earthquakes in the Tien Shan, central Asia, determined by P and SH waveform inversion, *J. Geophys. Res.*, **92**, 12,629–12,648, doi:10.1029/JB092iB12p12629.
- Nikonov, A. A. (1974), Contemporary and Holocene seismotectonic dislocations in the South Tien Shan seismically active zone (in Russian), *Izv. Akad. Sci. USSR Earth Phys.*, **12**, 71–76.
- Nikonov, A. A. (1975), An analysis of tectonic movements along the Hindu Kush-Darvaz-Karakul fault zone in Late Pliocene and Quaternary time (in Russian), *Bull. MOIP Geol. Sec.*, **50**(2), 5–23.
- Nikonov, A. A. (1977), *Holocene and Contemporary Movements of the Earth's Crust* (in Russian), 240 pp., Nauka, Moscow.
- Nikonov, A. A., A. V. Vakov, and I. A. Veselov (1983), *Seismotectonics and Earthquake Zones Near the Pamir and Tien Shan* (in Russian), 240 pp., Nauka, Moscow.
- Oreshin, S., L. Vinnik, D. Peregodov, and S. Roecker (2002), Lithosphere and asthenosphere of the Tien Shan imaged by S receiver functions, *Geophys. Res. Lett.*, **29**(8), 1191, doi:10.1029/2001GL014441.
- Pavlis, G. L., and S. Das (2000), The Pamir-Hindu Kush seismic zone as a strain marker for flow in the upper mantle, *Tectonics*, **19**, 103–115, doi:10.1029/1999TC900062.
- Peive, A. V., V. S. Burtman, S. V. Ruzhentsev, and A. I. Suvorov (1964), Tectonics of the Pamir-Himalayan sector of Asia, in *Report of the Twenty Second Session, India, International Geological Congress, Part XI: Himalayan and Alpine Orogeny*, edited by M. V. Muratov, pp. 441–464, Int. Geol. Congress, New Delhi.
- Reigber, C., G. W. Michel, R. Galas, D. Angermann, J. Klotz, J. Y. Chen, A. Papschev, R. Arslanov, V. E. Tzurkov, and M. C. Ishanov (2001), New space geodetic constraints on the distribution of deformation in central Asia, *Earth Planet. Sci. Lett.*, **191**, 157–165, doi:10.1016/S0012-821X(01)00414-9.
- Reilinger, R., et al. (2006), GPS constraints on continental deformation in the Africa-Arabia-Eurasia continental collision zone and implications for the dynamics of plate interactions, *J. Geophys. Res.*, **111**, B05411, doi:10.1029/2005JB004051.
- Richter, C. F. (1958), *Elementary Seismology*, 768 pp., W. H. Freeman, San Francisco, Calif.
- Roecker, S. W. (1982), Velocity structure of the Pamir-Hindu Kush region: Possible evidence for subducted crust, *J. Geophys. Res.*, **87**, 945–959, doi:10.1029/JB087iB02p00945.
- Roecker, S. W., T. M. Sabitova, L. P. Vinnik, Y. A. Burmakov, M. I. Golvanov, R. Mamatkanova, and L. Munirova (1993), Three-dimensional elastic wave velocity structure of the western and central Tien Shan, *J. Geophys. Res.*, **98**, 15,779–15,795, doi:10.1029/93JB01560.
- Ruzhentsev, S. V. (1963), Strike-slip faults of the southeastern Pamir, in *Faults and Horizontal Movements of the Earth's Crust* (in Russian), edited by A. V. Peive, *Tr. Geol. Inst. Akad. Nauk USSR*, **80**, 113–127.
- Sadybakasov, I. (1990), *Neotectonics of High Asia* (in Russian), 176 pp., Nauka, Moscow.
- Savarenskii, E. F., S. L. Solov'ev, and D. A. Kharin (1962), *Atlas of Earthquakes in the USSR: Results From Observed Networks of Seismic Stations of the USSR 1911–1957* (in Russian), 337 pp., Nauka, Moscow.
- Scharer, K. M., D. W. Burbank, J. Chen, R. J. Weldon, C. Rubin, R. Zhao, and J. Shen (2004), Detachment folding in the southwestern Tien Shan-Tarim foreland, China: Shortening estimates and rates, *J. Struct. Geol.*, **26**, 2119–2137, doi:10.1016/j.jsg.2004.02.016.
- Schwab, M., et al. (2004), Assembly of the Pamirs: Age and origin of magmatic belts from the southern Tien Shan to the southern Pamirs and their relation to Tibet, *Tectonics*, **23**, TC4002, doi:10.1029/2003TC001583.
- Shen, Z.-K., M. Wang, Y. Li, D. D. Jackson, A. Yin, D. Dong, and P. Fang (2001), Crustal deformation along the Altyn Tagh fault system, western China, from GPS, *J. Geophys. Res.*, **106**, 30,607–30,621, doi:10.1029/2001JB000349.
- Shultz, S. S. (1948), *Analysis of Neotectonics and Relief of the Tien Shan* (in Russian), 222 pp., OGIS, Moscow.
- Sinityn, N. M. (1960), *Tectonics of the Mountain Frame of Ferghana*, 218 pp., Leningrad Univ. Press, Leningrad, Russia.
- Sinityn, V. M. (1962), *Paleogeography of Asia*, 68 pp., Akad. Nauk, Moscow.
- Sobel, E. R., and T. A. Dumitru (1997), Thrusting and exhumation around the margins of the western Tarim Basin during the India-Asia collision, *J. Geophys. Res.*, **102**, 5043–5063, doi:10.1029/96JB03267.
- Sobel, E. R., M. Oskin, D. Burbank, and A. Mikolaichuk (2006a), Exhumation of basement-cored uplifts: Example of the Kyrgyz Range quantified with apatite fission track thermochronology, *Tectonics*, **25**, TC2008, doi:10.1029/2005TC001809.
- Sobel, E. R., J. Chen, and R. V. Heermann (2006b), Late Oligocene–Early Miocene initiation of shortening in the southwestern Chinese Tien Shan: Implications for Neogene shortening rate variations, *Earth Planet. Sci. Lett.*, **247**, 70–81, doi:10.1016/j.epsl.2006.03.048.
- Strecker, M. R., W. Frisch, M. W. Hamburger, L. Ratschbacher, S. Semiletin, A. Zamoruyev, and N. Sturchio (1995), Quaternary deformation in the eastern Pamirs, Tadjikistan and Kyrgyzstan, *Tectonics*, **14**, 1061–1079, doi:10.1029/95TC00927.
- Strecker, M. R., G. E. Hillel, J. R. Arrowsmith, and I. Coutand (2003), Differential structural and geomorphic mountain-front evolution in an active continental collision zone: The NW Pamir, southern Kyrgyzstan, *Geol. Soc. Am. Bull.*, **115**, 166–181, doi:10.1130/0016-7606(2003)115<0166:DSAGMF>2.0.CO;2.
- Sun, J., and Z. Zhang (2009), Syn-tectonic growth strata and implications for late Cenozoic tectonic uplift in the northern Tien Shan, China, *Tectonophysics*, **463**, 60–68, doi:10.1016/j.tecto.2008.09.008.
- Sun, J., R. Zhu, and J. Bowler (2004), Timing of the Tianshan Mountains uplift constrained by magnetostratigraphic analysis of molasse deposits, *Earth Planet. Sci. Lett.*, **219**, 239–253, doi:10.1016/S0012-821X(04)00008-1.
- Sun, J., Y. Li, Z. Zhang, and B. Fu (2009), Magnetotratigraphic data on Neogene growth folding in the foreland basin of the southern Tianshan Mountains, *Geology*, **37**, 1051–1054, doi:10.1130/G30278A.1.
- Tapponnier, P., and P. Molnar (1979), Active faulting and Cenozoic tectonics of the Tien Shan, Mongolia and Baykal regions, *J. Geophys. Res.*, **84**, 3425–3459, doi:10.1029/JB084iB07p03425.
- Thatcher, W. (2007), Microplate model for the present-day deformation of Tibet, *J. Geophys. Res.*, **112**, B01401, doi:10.1029/2005JB004244.
- Thomas, J.-C., H. Perroud, P. R. Cobbold, M. L. Bazhenov, V. S. Burtman, A. Chauvin, and E. Sadybakasov (1993), A paleomagnetic study of Tertiary formations from the Kyrgyz Tien-Shan and its tectonic implications, *J. Geophys. Res.*, **98**, 9571–9589, doi:10.1029/92JB02912.
- Thompson, S. C., R. J. Weldon, C. M. Rubin, K. Abdrakhmatov, P. Molnar, and G. W. Berger (2002), Late Quaternary slip rates across the central Tien Shan, Kyrgyzstan, central Asia, *J. Geophys. Res.*, **107**(B9), 2203, doi:10.1029/2001JB000596.
- Trifonov, V. G., V. Makarov, and S. F. Skobelev (1992), The Talas-Fergana active right-lateral fault, *Ann. Tecton.*, **6**, 224–237.
- Trifonov, V. G., E. V. Artjushkov, A. E. Dodonov, D. M. Bachmanov, A. V. Mikolaichuk, and F. A. Vishniakov (2008), Pliocene-Quaternary mountain-building in the central Tien Shan (in Russian), *Geol. Geofiz.*, **49**, 128–145.
- Ulomov, V. I. (1974), *Dynamics of the Earth's Crust and Prediction of Earthquakes* (in Russian), 214 pp., Fan, Tashkent.
- Vinnik, L. P., A. A. Lukk, and I. L. Nersesov (1977), Nature of the intermediate seismic zone in the mantle of the Pamirs—Hindu-Kush, *Tectonophysics*, **38**, T9–T14, doi:10.1016/0040-1951(77)90208-6.
- Vinnik, L. P., S. Roecker, G. L. Kosarev, S. I. Oreshin, and I. Y. Koulikov (2002), Crustal structure and dynamics of the Tien Shan, *Geophys. Res. Lett.*, **29**(22), 2047, doi:10.1029/2002GL015531.
- Wolfe, C. J., and F. L. Vernon III (1998), Shear-wave splitting at central Tien Shan: Evidence for rapid variation of anisotropic patterns, *Geophys. Res. Lett.*, **25**, 1217–1220, doi:10.1029/98GL00838.
- Yang, S., J. Li, and Q. Wang (2008), The deformation pattern and fault rate in the Tianshan Mountains inferred from GPS observations, *Sci. China Ser. D*, **51**, 1064–1080.
- Yin, A., S. Nie, P. Craig, T. M. Harrison, F. J. Ryerson, X. Qian Xianglin, and G. Yang (1998), Late Cenozoic tectonic evolution of the southern Chinese Tien Shan, *Tectonics*, **17**, 1–27, doi:10.1029/97TC03140.
- Zhu, B., W. S. F. Kidd, D. B. Rowley, B. S. Currie, and N. Shafique (2005), Age of initiation of the India-Asia collision in the east-central Himalaya, *J. Geol.*, **113**, 265–285, doi:10.1086/428805.
- Zubovich, A. V., V. I. Makarov, S. I. Kuzikov, O. I. Mosienko, and G. G. Schelochkov (2007), Intra-continental mountain building in central Asia as inferred from satellite geodetic data (in Russian), *Geotektonika*, **41**, 16–29. (*Geotectonics*, Engl. Transl., **41**, 13–25.)
- R. T. Beisenbaev, Seismological Experimental-Methodical Expedition, 050060, Almaty, Kazakhstan.
- V. D. Bragin, S. I. Kuzikov, and G. G. Schelochkov, Research Station of the Russian Academy of Sciences, 720049 Bishkek, Kyrgyzstan.
- Y. Dang, Chinese Academy of Surveying and Mapping, 100830 Beijing, China.
- B. H. Hager, T. A. Herring, and R. Reilinger, Department of Earth, Atmospheric, and Planetary Sciences, Massachusetts Institute of Technology, Cambridge, MA 02139, USA.
- M. W. Hamburger, Department of Geological Sciences, Indiana University, 1001 East 10th St., Bloomington, IN 47405-1405, USA.
- J. Li and X. Wang, Earthquake Administration of the Xinjiang Uygur Autonomous Region, 830011 Urumqi, China.
- V. I. Makarov, Institute of Environmental Geosciences, Russian Academy of Sciences, P.O. Box 145, Moscow, 101000, Russia.
- W. Michajljow and C. Reigber, Department 1, Deutsches GeoForschungsZentrum, Telegrafenberg, D-14473 Potsdam, Germany.
- P. Molnar, Department of Geological Sciences, University of Colorado, Boulder, CO 80309, USA. (peter.molnar@colorado.edu)
- O. I. Mosienko and A. V. Zubovich, Department of Technical Infrastructures and Data Management, Central Asian Institute for Applied Geosciences, 720027 Bishkek, Kyrgyzstan.
- Y. G. Scherba, National Center of Space Researches and Technologies, National Space Agency of the Republic of Kazakhstan, Shevchenko St. 15, 050010, Almaty, Kazakhstan.